High-Altitude Data Assimilation System Experiments for the Northern Summer Mesosphere Season of 2007

Stephen D. Eckermann[a,*] Karl W. Hoppel[b] Lawrence Coy[a]

John P. McCormack[a] David E. Siskind[a] Kim Nielsen[c]

Andrew Kochenash[c] Michael H. Stevens[a]

Christoph R. Englert[a] Mark Hervig[d]

[a] *Space Science Division, Naval Research Laboratory, Washington, DC*

[b] *Remote Sensing Division, Naval Research Laboratory, Washington, DC*

[c] *Computational Physics, Inc., Springfield, VA*

[d] *GATS, Inc., Driggs, ID*

Abstract

A global numerical weather prediction system is extended to mesospheric and lower thermospheric altitudes and used to assimilate high-altitude satellite measurements of temperature, water vapor and ozone from MLS and SABER during May-July 2007. Assimilated temperatures from 100-0.001 hPa show minimal biases compared to satellite data and existing analysis fields. Saturation ratios derived diagnostically from assimilated temperature and water vapor fields at PMC altitudes and latitudes compare well with seasonal variations in PMC frequency derived from measurements from the Aeronomy of Ice in the Mesosphere (AIM) satellite. Synoptic maps of these diagnostic saturation ratios correlate geographically with three independent transient mesospheric cloud events observed at mid-latitudes by SHIMMER on STPSat-1 and by ground observers during June 2007. Assimilated temperatures and winds reveal broadly realistic amplitudes of the quasi 5-day wave and migrating tides as a function of latitude and height. The 5-day wave and migrating diurnal tide also produce water vapor responses in the polar summer MLT. These features do not correlate linearly with corresponding temperature amplitudes and thus may have a more complex origin than the 5-day wave response in PMC brightness.

Key words:
data assimilation, polar mesospheric clouds

1 Introduction

Global numerical weather prediction (NWP) systems consist of two main components: a forecast model that predicts future atmospheric conditions, and a data assimilation system (DAS) that provides global initial conditions for those forecasts based on available observations. The quality of these operationally assimilated fields, and hence the skill of the resulting forecasts, rely heavily on the high-density planetary-scale measurements provided from satellites.

The maturity and sophistication of NWP DASs have now led them to directly assimilate satellite radiances, since the forecast models now provide more accurate *a priori* estimates than the climatologies typically used in standard

* corresponding author: c/- Code 7646, Space Science Division, Naval Research Laboratory, 4555 Overlook Ave. SW, Washington, DC, 20375, USA. Tel: +1-202-404-1299; FAX: +1-202-404-8090; email: stephen.eckermann@nrl.navy.mil

satellite retrievals. Radiance weighting functions, however, are typically vertically broad, with some having long "tails" that extend to high altitudes not covered by the forecast model component. This latter restriction reduces the accuracy of the radiance assimilation, and can prevent certain channels from being assimilated. Thus most operational centers are progressively increasing the vertical range of their NWP systems to span most of the stratosphere, with a few now extending into the lower mesosphere.

To date, however, no operational NWP system extends through the mesosphere and lower thermosphere (MLT), due primarily to a lack of operational radiance channels in this altitude range. This is changing with the launch of the latest generation of operational sensors, such as the Special Sensor Microwave Imager/Sounder (SSMIS) (Lipton, 2002; Kerola, 2006), and the advent of fast radiative transfer codes suitable for assimilating MLT radiances operationally (Han et al., 2007). Thus research NWP systems extending into the MLT are now being actively developed (Polavarapu et al., 2005a; Hoppel et al., 2008). Since the boundary between atmosphere and space is defined arbitrarily at an MLT altitude of either 80 or 100 km, such systems represent the first steps towards a truly integrated global ground-to-space forecasting capability. Here we work with one such developmental ground-to-MLT NWP system: the Advanced Level Physics High-Altitude (ALPHA) prototype of the Navy Operational Global Atmospheric Prediction System (NOGAPS), which we describe in section 2.

Adding an MLT component to an NWP system presents a variety of technical challenges that are only just beginning to be grappled with. The vertically extended forecast model must include new physical processes appropriate for the MLT: those for NOGAPS-ALPHA are discussed in section 2.1. Coupling the forecast model to the DAS raises further issues, such as vertical information transfer, model-data biases, appropriate dynamical balance constraints, and resolved and parameterized gravity wave dynamics (Polavarapu et al., 2005b; Sankey et al., 2007). In developing and testing new MLT components, research MLT data, such as provided by the Aeronomy of Ice in the Mesosphere (AIM) satellite (Russell et al., 2008), are particularly valuable, either for direct assimilation into the system or for independent validation of MLT DAS output.

Research satellites typically measure only a targeted subset of atmospheric parameters specific to their core science objectives, usually within a limited range of longitudes, latitudes, heights and local times. AIM, for example, consists of the Solar Occultation for Ice Experiment (SOFIE), which performs limb occulation measurements of temperature and constituents at a fixed local time (Gordley et al., 2008), and the Cloud Imaging and Particle Size (CIPS) instrument, which images polar mesospheric cloud (PMC) properties in the vertical (McLintock et al., 2008). By contrast, NWP systems can assimilate data from a range of satellite and suborbital instruments to provide an optimal global state estimate, filling any spatial or temporal gaps using the global model's full-physics forecast fields constrained by DAS-based initial conditions. The synoptic gridded analysis products that result are more amenable to research studies, while providing a range of other atmospheric parameters that may not be measured directly (e.g., winds). The scientific value of such DAS products for NASA's middle atmosphere satellite research missions is already well established. Global analysis fields generated by the Met Office DAS, for instance, played a pivotal role in science studies based on data from the Upper Atmosphere Research Satellite (UARS), while NASA's Global Modeling and

Assimilation Office (GMAO) GEOS DAS analyses are central to all aspects of the current Aura and Aqua missions (see, e.g., Susskind et al., 2006; Manney et al., 2007). Thus one motivation for the present work is to generate synoptic analysis fields extending into the MLT that provide analogous support for AIM.

There are many ways in which ground-to-MLT DAS fields could contribute to the science return from AIM. For example, there is debate as to the role of vertical and latitudinal tidal and planetary wave transport in controlling PMC variability (e.g., Berger and vonZahn, 2007; Gerding et al., 2007; Stevens et al., 2008). The limited local time coverage of satellite MLT measurements, however, presents well-known difficulties in isolating mean, tidal and fast planetary wave signatures. Data analysis studies to date have employed complex asynoptic mapping or least-squares fitting algorithms that require assumptions about stationarity, aliasing and seasonal dependences (e.g., Wu et al., 1995; Burrage et al., 1995; Forbes et al., 1997; Zhu et al., 2005). While these assumptions can be tested and the procedures improved with the help of MLT fields from general circulation models (Oberheide et al., 2003; McLandress and Zhang, 2007) and addition of data from other instruments (Drob et al., 2000; Azeem et al., 2000), final mean mesospheric temperature estimates from these algorithms can still have large uncertainties (Drob et al., 2000; Oberheide et al., 2003; Zhu et al., 2005). NWP systems combine aspects of all the aforementioned algorithms by optimally assimilating MLT data from a variety of sources with the aid of a full-physics general circulation model (GCM) to constrain the system dynamically and optimally fill gaps. The physical and dynamical constraints of the system yield additional benefits, such as estimates of atmospheric parameters not directly measured, such as winds. Furthermore, mean and root-mean-square (RMS) differences between the model forecasts (F), observations (O) and the analysis fields (A) provide objective quantification of the inherent biases and uncertainties of all the analyzed physical quantities output by the system.

We explore these potential benefits for MLT science in this paper. After describing the system in section 2 and tuning it in section 3, we validate its output against independent observations and analysis fields in section 4. In section 5 we study the seasonal variation of temperature and water vapor at PMC altitudes from the NOGAPS-ALPHA analysis and compare with corresponding PMC data acquired from AIM. Section 6 studies planetary wave signals in the analysis fields, focusing on the quasi 5-day wave and solar migrating tides near PMC regions. Section 7 applies the synoptic analysis fields to mid-latitude mesospheric cloud events reported at specific geographical locations on specific dates. Section 8 summarizes the major findings of these assimilation experiments and assesses near-term development needs for the system to improve MLT products in future assimilation experiments.

2 NOGAPS-ALPHA

Here we briefly describe the salient aspects of the NOGAPS-ALPHA system used in this study. Hoppel et al. (2008) provide a complete overview of the initial system developed for data assimilation research.

2.1 Forecast Model Component

Hogan and Rosmond (1991) and Hogan et al. (1991) provide detailed descriptions of the NOGAPS global forecast model. Briefly, the dynamical core is Eulerian, hydrostatic, spectral in the horizontal and finite difference in the vertical, using the specific Lorenz-grid vertical discretization of Arakawa and Suarez (1983) generalized to hybrid vertical coordinates following Simmons and Burridge (1981). The model is forwarded using a three time-level scheme incorporating a semi-implicit treatment of gravity wave propagation, implicit zonal advection of moisture and constituents, and Robert (Asselin) time filtering. The operational model's physical parameterizations include vertical diffusive transport in the planetary boundary layer (Louis, 1979; Louis et al., 1982) coupled to a land surface model (Hogan, 2007), orographic gravity-wave and flow-blocking drag (Webster et al., 2003), shallow cumulus mixing (Tiedtke, 1984), deep cumulus convection (Peng et al., 2004), convective, stratiform and boundary layer clouds and precipitation (Slingo, 1987; Teixeira and Hogan, 2002), and shortwave and longwave radiation (Harshvardhan et al., 1987). At the Fleet Numerical Meteorological and Oceanographic Center (FNMOC) NOGAPS runs operationally at T239L30 (T119L30 for ensemble forecasts) using mean orography, pure σ levels, a rigid upper boundary at p_{top} =1 hPa and layer thicknesses that yield a highest undiffused model layer at $\sim$25 hPa.

The progressive extension of this forecast model through the stratosphere and into the lower mesosphere for NOGAPS-ALPHA has been described by Eckermann et al. (2004) and Allen et al. (2006). We briefly summarize salient additions here, focusing mostly on new physical parameterizations required to forecast the MLT and support the DAS at these altitudes.

2.1.1 *Radiation*

The high-altitude forecast model has been designed to switch easily between any of the operational or research physics packages. Thus, while the operational Harshvardhan et al. (1987) radiation schemes can be used, NOGAPS-ALPHA runs here use different schemes that extend to MLT altitudes. Radiative heating rates are computed using the Chou and Suarez (1999) scheme. We deactivate their near-infrared (IR) CO_2 band contributions at upper levels and use instead upper-level rates from Fomichev et al. (2004) that better parameterize non-local thermodynamic equilibrium (non-LTE) effects on these near-IR bands. Longwave cooling rates are computed using the parameterization of Chou et al. (2001), which is accurate from the ground to 0.01 hPa, and of Fomichev et al. (1998), which includes non-LTE effects on IR CO_2 emissions at MLT altitudes. The two profiles $Q_{Chou}(Z)$ and $Q_{Fomichev}(Z)$ are blended into a final cooling rate profile

$$Q(Z) = w(Z)Q_{Chou}(Z) + [1 - w(Z)]\, Q_{Fomichev}(Z), \tag{1}$$

using a pressure-height dependent linear weight

$$w(Z) = \frac{1 - \tanh\left(\frac{Z - Z_{int}}{\zeta}\right)}{2}, \tag{2}$$

where Z_{int} =75 km and ζ =5 km. Due to the computational expense, here we update radiative heating and cooling rates every 2 hours.

2.1.2 *Trace Constituents*

Specific humidity q is built into the discretized NOGAPS primitive equations through the virtual potential temperature. Thus NOGAPS-ALPHA must initialize and forecast it accurately from the surface to the MLT. In addition to NOGAPS tropospheric moist physics parameterizations, we have developed new parameterizations of water vapor production in the stratosphere due to methane oxidation and photolytic loss in the mesosphere (McCormack et al., 2008). However, as the rates are generally slow except at the very highest altitudes, they were not used in the data-assimilation runs reported here, so that middle atmospheric water vapor was simply advected passively by the forecast model. Only prognostic q values below 200 hPa altitude are used in the radiation calculations: above that, values from observational and model-based climatologies are used (see section 3.1.1.1 of Eckermann et al., 2007, for details).

The forecast model incorporates a new prognostic capability for ozone, with a number of ozone photochemistry parameterizations available for use (Eckermann et al., 2004; McCormack et al., 2004). Here we use the scheme of McCormack et al. (2006) that is run operationally in the National Centers for Environmental Prediction Global Forecast System (NCEP GFS). It uses lookup tables of diurnally averaged photochemical coefficients derived from a full chemistry model based on linearizing scaled odd-oxygen production and loss rates about equilibrium states. These equilibrium states are specified in the model using zonal-mean observational climatologies, and are chosen carefully here to match characteristics of the assimilated ozone observations so as to avoid model-data bias (Geer et al., 2007; Coy et al., 2007). The scheme does not at present parameterize either diurnal ozone photochemistry at altitudes above $\sim$0.3 hPa or tropospheric ozone chemistry, relaxing ozone in both altitude regions to a reference state based on a mean photochemical relaxation rate. Because of this, here we do not use prognostic ozone mixing ratios χ_{O3} in the radiation calculations. Instead we use the observational ozone climatology described by Eckermann et al. (2007) that incorporates daytime ozone data only at high altitudes. That climatology was improved slightly here by adding high-altitude daytime ozone data from the High Resolution Doppler Imager (Marsh et al., 2002) at the very highest altitudes. These daytime ozone climatologies improve the model's radiative heating rates (Eckermann et al., 2007) which are important for accurately modeling and assimilating temperature at these altitudes (e.g., Sassi et al., 2005). For simplicity, the night-to-day ratio used by Eckermann et al. (2007) to scale up nighttime ozone values for the cooling rate calculations was not used since it is a more minor effect for temperature prediction.

2.1.3 Gravity Wave Drag

Nonorographic gravity wave drag (GWD) is the most important new parameterization required for summer MLT prediction (e.g., Fritts and Luo, 1995). Here we use a multiwave scheme based on the linear GW saturation formulation of Lindzen (1981), as developed for the Whole Atmosphere Community Climate Model (WACCM). Appendix A of Garcia et al. (2007) provides a detailed description. Here we summarize the important aspects for the present work.

The scheme launches a prescribed spectrum of n_{gw} individual GWs within every grid box at a source level set here to 500 hPa (following Garcia et al., 2007). Each GW j is assigned a unique ground-based horizontal phase speed

$$\begin{aligned} c_j &= |U_{500}| + j\Delta c, \\ j &= -n_c, -n_c+1, \ldots + n_c - 1, +n_c, (j \in \mathbf{Z}, n_c \in \mathbf{N}), \end{aligned} \tag{3}$$

such that phase speeds are distributed symmetrically with respect to the 500 hPa horizontal wind speed $|U_{500}|$. As in Garcia et al. (2007) we choose Δc =2.5 m s^{-1} and n_c =32, yielding $n_{gw} = 2n_c + 1$ =65 component gravity waves with intrinsic phase speeds $|c_j - U_{500}|$ distributed between $\pm$80 m s^{-1}, all aligned along the 500 hPa wind speed direction. The vertical flux of horizontal pseudomomentum density (Eliassen-Palm flux) of each wave, $\tau_{src}(c_j)$, is assigned based on a Gaussian flux distribution versus phase speed, centered about $|U_{500}|$, of the form

$$\tau_{src}(c_j) = \tau_b F(\phi, t) \exp\left[\frac{-\left(c_j - c_{j=0}\right)^2}{\hat{c}_w^2}\right]. \qquad (4)$$

Following Garcia et al. (2007) we set the phase-speed width $\hat{c}_w$ =30 m s^{-1} and tune the so-called background flux τ_b in experiments described in section 3. The function $F(\phi, t)$, plotted in Figure 1, is an analytical fit as a function of latitude ϕ and time (month) t to results obtained from diagnostically processing long-term climate model output using a proposed parameterization of frontogenetic gravity wave generation (c.f. Figure 2 of Charron and Manzini, 2002). It yields a large winter-summer flux asymmetry in each hemisphere as well as a gradual variation during the season: see Garcia et al. (2007) for further details.

Wave propagation, wave breaking and saturation, and resulting diffusive and thermal dissipation of wave momentum flux are modeled for each wave as in Garcia et al. (2007). At model layer k, the ensuing GW-induced mean-flow acceleration due to wave j is

$$a_{j,k} = -g\epsilon \frac{\partial \tau_{j,k}}{\partial p}, \qquad (5)$$

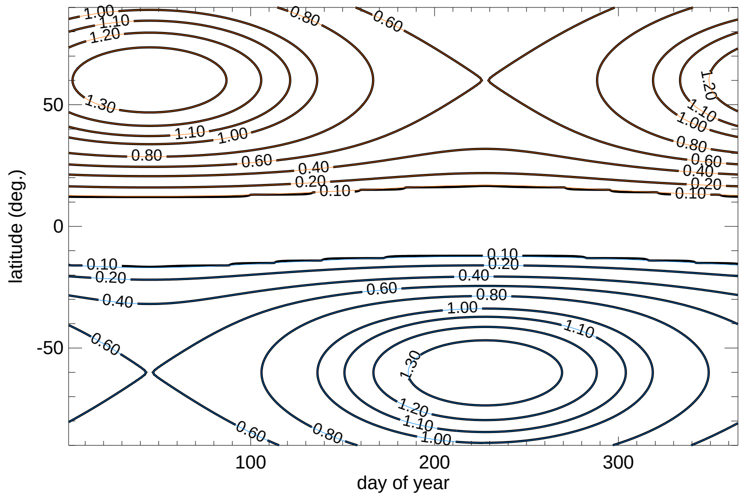

Fig. 1. GWD source function $F(\phi, t)$. Orange and blue contours show its northern and southern hemisphere components, respectively.

where g is gravitational acceleration and p is pressure. This acceleration, directed along the 500 hPa (source-level) wind speed direction, is apportioned to modify zonal and meridional wind speeds accordingly, and summed over all GWs j. All remaining flux is deposited in the top two model layers to conserve momentum so as to capture robust downward-control responses (Shaw and Shepherd, 2007).

The factor ϵ in (5) is a constant set in the range $0 \leq \epsilon \leq 1$. Such normalization terms occur routinely in Lindzen-type schemes to ameliorate excessively large and/or insufficiently smooth GWD in models, and are usually justified physically as encapsulating either the net "efficiency" of wave breaking or the net "intermittency" of GW activity, either in time (due to variable forcing) or spatially due to incomplete filling of the grid box by the GW packets. The mathematical implementation of the efficiency concept in (5), which follows that used in the Alexander and Dunkerton (1999) scheme, simply scales down all the GWD values by a constant amount. It should be noted that similar efficiency factors are implemented in different ways mathematically in other Lindzen schemes, where they act differently and modify both the shape and magnitude of the GWD profile (Hamilton, 1997; McLandress, 1998; Norton and Thuburn, 1999). The specific implementation here has the practical advantage that source flux parameters like τ_b can be adjusted to modify the shape of the GWD profile, whereupon ϵ can then be adjusted to scale the final GWD while retaining the tuned profile shape. Specific GWD tuning for the NOGAPS-ALPHA assimilation runs is discussed in section 3.

For the experiments reported here, we apply only the scheme's GW momentum flux divergence tendencies to the model: GWD-induced vertical diffusivities, while calculated, are not at present used to mix momentum, heat or constituents in the model. Orographic GWD is applied separately using either a Palmer et al. (1986) or Webster et al. (2003) scheme: we choose the former here following Siskind et al. (2007).

2.1.4 Resolution and Height Range

As in Hoppel et al. (2008) the forecast model is run here at a triangular spectral truncation of T79, corresponding to 1.5° longitude resolution on the quadratic Gaussian grid. We use 68 model layers that extend into the MLT (p_{top} =5 10^{-4} hPa) with a vertical pressure height resolution ΔZ ≈2 km throughout the middle atmosphere. The runs here use the "NEWHYB2" hybrid vertical coordinate described by Eckermann (2008) with k_p =43 isobaric model layers between p_{top} and $p_{k_p+1/2}$ ∼87.4 hPa. This new hybrid coordinate reduces vertical truncation errors in the stratosphere and MLT (Eckermann, 2008) and should improve the quality of the assimilations above the tropopause (see, e.g., Trenberth and Stepaniak, 2002).

2.2 DAS Component

The NOGAPS-ALPHA DAS uses a three-dimensional variational (3DVAR) algorithm formulated in observational space, known as the Naval Research Laboratory (NRL) Atmospheric Variational DAS, or NAVDAS. The basic formulation and initial performance are described by Daley and Barker (2001a), while Daley and Barker (2001b) provide a more detailed description. Hoppel et al. (2008) explain how NAVDAS was interfaced to the NOGAPS-ALPHA forecast model to run as a coupled NWP system extending into the MLT. The version and setup used here are very similar to those described by Hoppel et al. (2008), and so we focus here mainly on an overview of that system and salient differences for the experiments reported here.

Given a column vector $\mathbf{x_b}$ containing I "background" estimates of some atmospheric parameter (e.g., temperature) and L estimates of some related observation $\mathbf{y}$ (e.g., thermal radiance), NAVDAS generates a corresponding analysis vector $\mathbf{x_a}$ by numerically minimizing the scalar cost function

$$J(\mathbf{x_a}) = (\mathbf{y} - \mathcal{H}(\mathbf{x_a}))^T \, \mathbf{R}^{-1} \, (\mathbf{y} - \mathcal{H}(\mathbf{x_a})) + (\mathbf{x_b} - \mathbf{x_a})^T \, \mathbf{P_b}^{-1} \, (\mathbf{x_b} - \mathbf{x_a}) \,. \quad (6)$$

Here $\mathcal{H}$ is the forward observation operator (e.g., a radiative transfer forward model that converts temperature into radiance) and $\mathbf{R}$ is the $L \times L$ error covariance matrix of this conversion: similarly $\mathbf{P_b}$ is the $I \times I$ error covariance matrix in the background estimate, and T denotes transpose. (6) is identical in form to cost functions solved in standard satellite retrievals except here the background $\mathbf{x_b}$ is provided by the forecast model.

The observation-space solution to (6) is (Daley and Barker, 2001a)

$$\mathbf{x_a} - \mathbf{x_b} = \mathbf{P_b}\mathbf{H}^T \left[\mathbf{H}\mathbf{P_b}\mathbf{H}^T + \mathbf{R}\right] \left[\mathbf{y} - \mathcal{H}(\mathbf{x_b})\right], \tag{7}$$

which converts the so-called innovations $\mathbf{y} - \mathcal{H}(\mathbf{x_b})$ in the observation space into a correction vector $\mathbf{x_a} - \mathbf{x_b}$ in model/analysis space. The matrix $\mathbf{H} = \partial\mathcal{H}/\partial\mathbf{x}|_{\mathbf{x_b}}$ originates as an approximation of $\mathcal{H}(\mathbf{x_a})$ by the truncated Taylor series expansion $\mathcal{H}(\mathbf{x_b}) + \mathbf{H}[\mathbf{x_a} - \mathbf{x_b}]$. The accuracy of this approximation, and hence the quality of the analysis, clearly requires *inter alia* that $\mathbf{x_a} - \mathbf{x_b}$ be as small as possible, and thus that the forecast model be minimally biased with respect to both observations and analysis (see section 3).

Research forecast-assimilation runs with NOGAPS-ALPHA use the archived sensor data routinely assimilated operationally by NOGAPS at FNMOC (see Table 1 of Baker et al., 2007). Most relevant here for the middle atmosphere are Advanced Microwave Sounding Unit (AMSU-A) thermal radiances from stratospheric channels 9 and 10 on the NOAA-15 and NOAA-16 satellites. We use the NAVDAS operational data-thinning schemes for these radiances described by Baker et al. (2005).

In the initial NOGAPS-ALPHA implementation, Hoppel et al. (2008) assimilated limb-scanned temperature data from:

- the Microwave Limb Sounder (MLS) on Aura from 32-0.01 hPa (version 2.2 retrievals: see Schwartz et al., 2008);
- the Sounding of the Atmosphere Using Broadband Emission Radiometry (SABER) instrument on the Thermosphere Ionosphere Mesosphere Energetics and Dynamics (TIMED) satellite from 32-0.019 hPa (version 1.06 retrievals: see Mertens et al., 2004).

In this study we also assimilate SABER and MLS temperatures using the same observation operators and error covariances for these instruments described by Hoppel et al. (2008). Here, however, we use version 1.07 SABER retrievals that account for the vibrational exchange between CO_2 isotopes. Kutepov et al. (2006) have shown that this process is critical for getting reliable temperatures in the summer mesopause.

Here we assimilate SABER and MLS temperatures up to a higher altitude of 0.002 hPa, in order to insert data at polar summer mesopause altitudes. As in Hoppel et al. (2008) the increments above this top data insertion level are progressively damped over a ∼6 km pressure height range, before reverting thereafter to pure forecast fields. Hoppel et al. (2008) fitted and removed a global mean profile of the bias between SABER and MLS temperatures, using the latter as truth to bias correct the SABER data. The calculation is repeated here for the May-June period using the version 1.07 SABER data over this higher altitude range. The resulting bias profile in Figure 2 is similar to independent estimates of both Hoppel et al. (2008) and Schwartz et al. (2008).

PMC formation and microphysics depend sensitively on not just temperature but water vapor abundances, which in turn depend on HO_x/O_x chemistry. Thus in these experiments we also assimilate version 2.2 MLS retrievals of χ_{H_2O} and χ_{O_3}.

Lambert et al. (2007) and Read et al. (2007) provide detailed descriptions and validation of the version 2.2 MLS χ_{H_2O} retrievals at upper and lower altitudes, respectively. They recommend that science studies using these data be confined to the 316-0.002 hPa range. Here we assimilate MLS χ_{H_2O} profiles

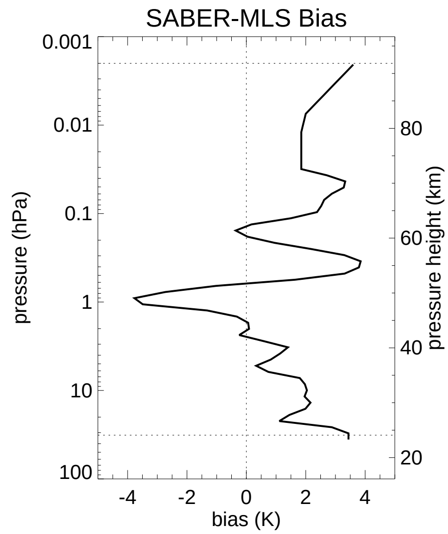

Fig. 2. Global-mean bias of SABER using MLS as truth, estimated using O-F statistics from the test assimilation (15 May-20 June) following Hoppel et al. (2008). Upper and lower limits of data insertion are marked with dotted lines.

from 220-0.002 hPa. We use horizontal correlation lengths of 358 km for these data, consistent with consensus values in Table 2 of Lambert et al. (2007). The effective vertical resolution of these data increase with altitude but, as for MLS temperatures, we use a constant mean vertical Gaussian averaging with a full-width half-maximum (FWHM) of ∼4 km: more detailed discussion of these choices is provided in section 3.2 of Hoppel et al. (2008).

We assimilate MLS χ_{O_3} profiles from 215-0.02 hPa, the same validated range quoted in Table 1 of Jiang et al. (2007), who showed good agreement with sub-orbital ozone profiles throughout the middle atmosphere. Since the forecast model does not parameterize diurnal ozone photochemistry (see section 2.1), we assimilate only daytime values at altitudes above 1 hPa. The vertical resolution of the data is ∼3 km throughout the range, which we use as our vertical averaging FWHM for these data in the DAS along with the same horizontal correlation lengths as for MLS temperature of ∼380 km.

The system runs in a standard 6-hour forecast-assimilation cycle, which presents challenges for assimilating tides (Swinbank et al., 1999): given their importance in the MLT, the following choices were made to aid assimilation of tidal features. The standard nonlinear normal mode initialization (NNMI) of the analysis state by the forecast model was deactivated, given that it mishandles migrating tides (Wergen, 1989). NOGAPS-ALPHA can perform NNMI on the analysis increments only, which treats tides at lower altitudes much better while still eliminating gravity wave noise (Ballish et al., 1992; Seaman et al., 1995). However, since its potential impact at new MLT altitudes has not been methodically investigated, we opted to deactivate it too and thus perform no initial-state filtering of the analysis prior to running forecasts. Work by Sankey et al. (2007) with the Canadian Middle Atmosphere Model (CMAM) suggests that the additional resulting GW noise in the forecast can propagate into the MLT and break, affecting mean and tidal structures, with some damping of tidal amplitude and spreading of tidal frequencies: nonetheless, their work indicates that broadly realistic diurnal and semidiurnal tides are still captured in the MLT analysis fields.

3 Reduction of Model Bias By Tuning the GWD Parameterization

Biases in model forecasts yield biased analysis fields (Dee and daSilva, 1998). Thus, prior to commencing the assimilation runs reported here, we performed an iterative series of 2-week forecasts that were initialized to high-altitudes at various times in June 2007 using output from a one-month test assimilation. The forecasts of zonal-mean temperature were compared with time series of MLS and SABER zonal-mean temperatures at various latitudes and pressures. These comparisons led to adjustment of the background flux τ_b and/or efficiency ϵ used in the nonorographic GWD scheme (see section 2.1.3), whereupon the forecasts and comparisons were repeated until the forecast temperatures were close to the observations throughout June, focusing especially on the polar summer MLT.

The top four panels in Figure 3 summarize results of four different forecast experiments each initialized on 1 June, showing zonal-mean summer hemisphere temperatures after +14 days. Forecasts in Figure 3a used the default τ_b and ϵ settings of Hoppel et al. (2008) and yield a polar summer mesopause that is located too low in altitude, followed by an unrealistically sharp temperature gradient yielding a thin warm layer at ~0.002 hPa: zonal-mean MLS temperatures on 15 June 2007 are shown for reference in Figure 3f. Reducing τ_b by a factor of 4 to 1.75 mPa yields forecast temperatures in Figure 3b that all but eliminate the secondary warm layer and generate a polar summer mesopause at roughly the right altitude, but which is too warm relative to MLS and SABER. Increasing ϵ by a factor of 2 yields an excessively cold mesopause (Figure 3c). An intermediate choice of ϵ =0.0175 yields zonal-mean forecast temperatures in Figure 3d with a polar summer mesopause of about the right altitude and temperature according to both SABER and MLS. Forecasts initialized at other times in June produce similarly good results using these settings (see, e.g., Figure 3e).

Changes in τ_b and ϵ above apply globally to reduce GWD in the winter (southern) hemisphere as well, where they yield forecast temperatures that compare less favorably with MLS and SABER due to reduced diabatic descent. Thus we performed aditional forecasts that retained the tuned summer GWD settings in Figure 3d but increased winter GWD by scaling up $F(\phi, t)$ in the south

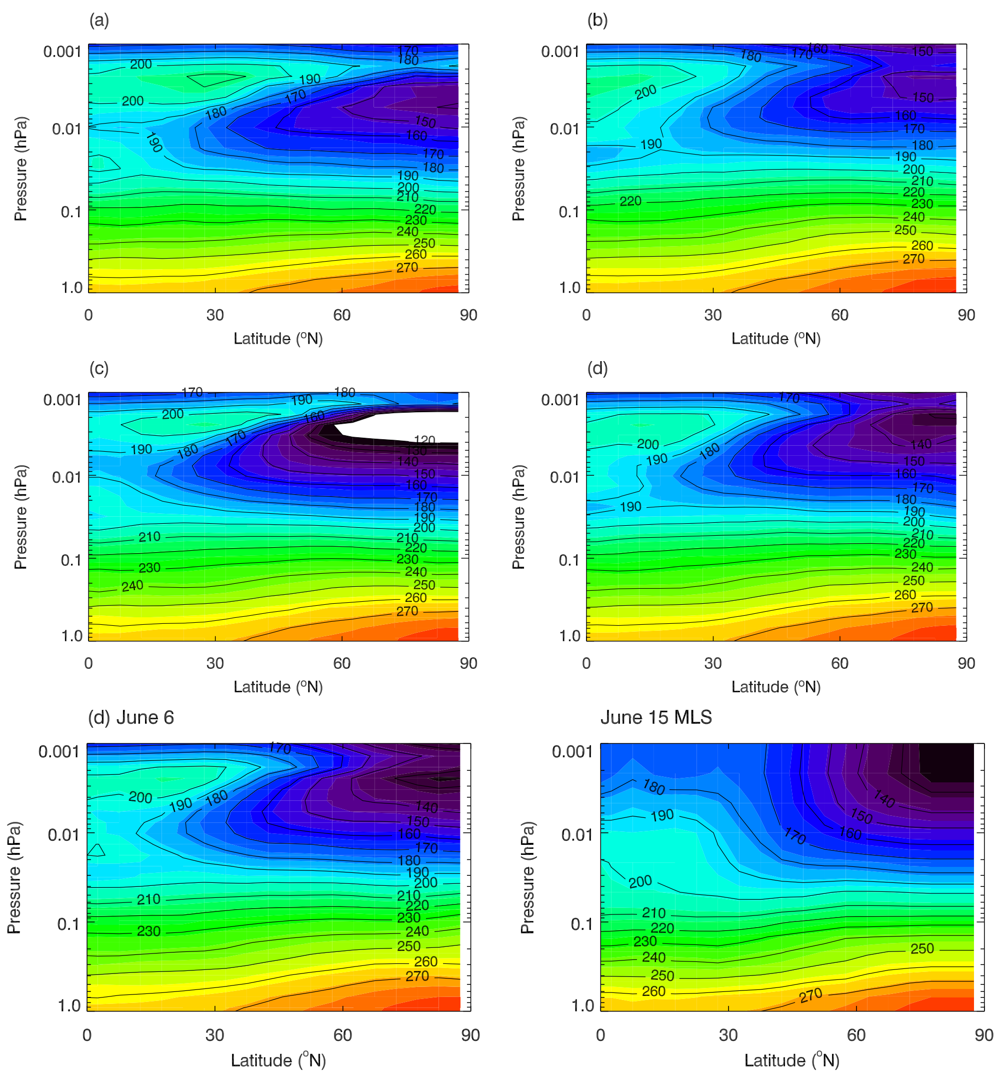

Fig. 3. Zonal-mean northern-hemisphere temperatures from 1-0.001 hPa of four NOGAPS-ALPHA +14 day forecasts, initialized on 1 June 2007 using preliminary high-altitude analysis fields and the following nonorographic GWD parameter settings: (a) $\tau_b = 7$ mPa, $\epsilon = 0.0125$; (b) $\tau_b = 1.75$ mPa, $\epsilon = 0.0125$; (c) $\tau_b = 1.75$ mPa, $\epsilon = 0.0250$; (d) $\tau_b = 1.75$ mPa, $\epsilon = 0.0175$. Panel (e) shows results using same settings as (d) but initialized on 6 June. Panel (f) shows zonal-mean MLS temperatures on 15 June. Temperatures below 120 K are not plotted.

(blue curve in Figure 1). A series of these experiments (not shown) yielded summer MLT forecasts consistently poorer than Figure 3d, due to the indirect effects of increased winter GWD on summer MLT temperatures through a modified mesospheric residual circulation (Becker and Fritts, 2006). Thus we settled here upon tuned GWD settings of τ_b =1.75 mPa and ϵ =0.0175 for our final assimilation run to reduce the potential for large mean O-F (innovation) biases in the summer MLT, with the understanding that forecast biases may be more significant in the winter hemisphere in these runs.

4 Initial Validation

The final assimilation run that was subsequently performed extends over nearly a full PMC season, from 15 May 2007 to 10 August 2007. However, on 15 July the TIMED satellite yawed so that SABER no longer measured the polar summer MLT. Thus, hereafter we analyze results only up to $\sim$15 July, during which both MLS and SABER were each contributing data to the polar summer MLT assimilation. The system generates regularly gridded global analysis fields of geopotential heights, temperatures, water vapor and ozone mixing ratios, horizontal winds, and other quantities every 6 hours at 60 reference pressure levels distributed roughly evenly in pressure height over the range 1000–0.0005 hPa.

As the assimilation proceeded, quality checks were performed by comparing zonal-mean temperature output with separate MLS and SABER zonal means computed from 2 days of data. While MLS and SABER each provide good global coverage over 2 days, their local time sampling is limited and different. Figures 4 and 5 plot examples of such comparisons for 24 June 2007. Differences are plotted in the lower panel of these figures, and are all generally small at altitudes below $\sim$0.01 hPa.

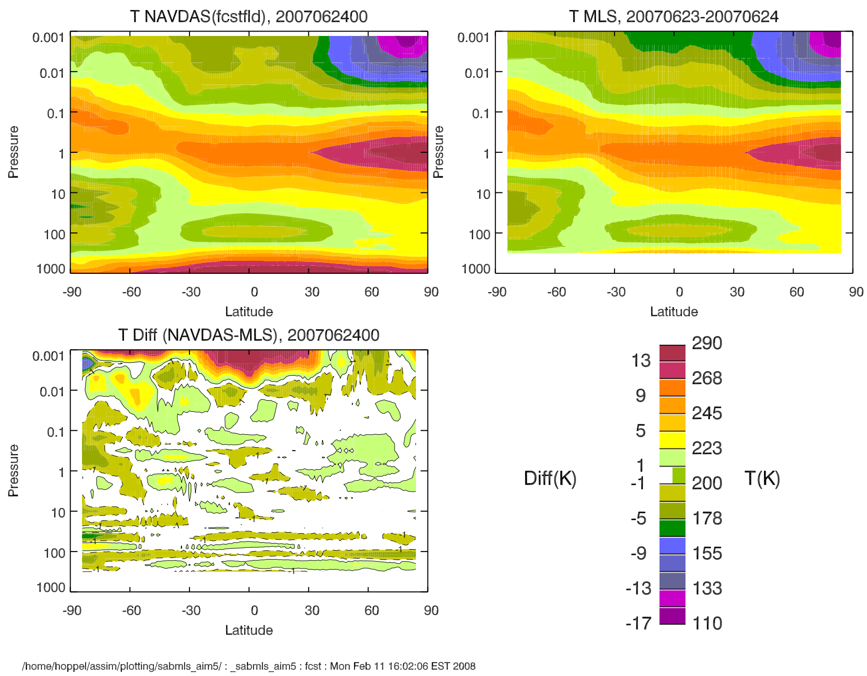

Fig. 4. Zonal-mean temperatures from (a) NOGAPS-ALPHA analysis on 24 June 2007, (b) MLS on 23-24 June 2007, and (c) differences between (a) and (b).

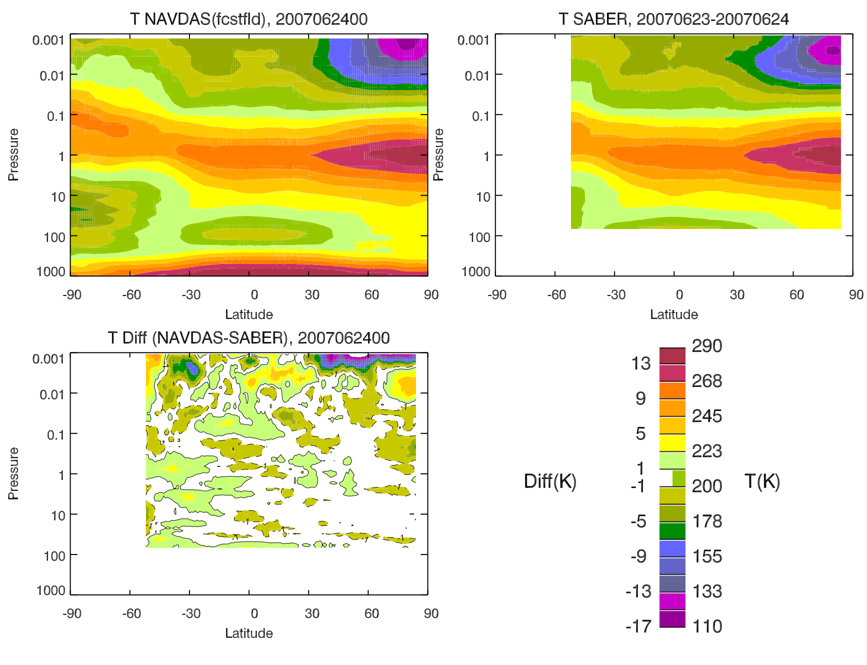

Fig. 5. Same presentation as Figure 4 but using SABER temperatures instead of MLS.

At higher altitudes Figure 4 shows a warm bias relative to MLS at the equator and subtropics that is not seen in the SABER comparison in Figure 5. The feature is too broad latitudinally and too stationary in time to be explained by aliasing of the diurnal tide, and seems to reflect systematic biases between the two measurements, highlighting potential weaknesses in our use of a single bias correction profile in Figure 2. Since MLS averaging kernels become vertically broad here, our use of constant vertical averaging widths for MLS data in the DAS may also be problematic. Additionally, the forecast model does not reproduce a realistic semiannual oscillation of the equatorial MLT with the current GWD settings due to insufficient tropical GW flux, an issue currently being addressed separately by tropical GWD tuning experiments over climate time scales with the forecast model.

The SABER comparisons in Figure 5 show a systematic warm bias at the uppermost polar summer MLT altitudes that is not seen in the MLS comparisons. Kutepov et al. (2006) note that a residual warm bias in version 1.07 SABER temperatures may still exist above $\sim$86 km altitude in polar summer. However, the bias here could instead reflect cold biases in MLS at these altitudes like those seen at other latitudes in Figure 4. If borne out, then future bias correction schemes may be needed that apply separately to both MLS and SABER. Overall, however, these comparisons reveal consistency among MLS, SABER and analyzed temperatures at most altitudes, including at and just below summer mesopause altitudes where PMCs form.

Next we compared assimilated fields with preliminary retrievals from SOFIE. These comparisons serve two purposes. First, as measurements not assimilated into the system, SOFIE data provide independent validation of the analysis. Second, SOFIE retrievals are at an early stage of development, and can themselves benefit from validation studies. Thus, these comparisons should be viewed as mutual cross-validation of two independent emerging AIM-related

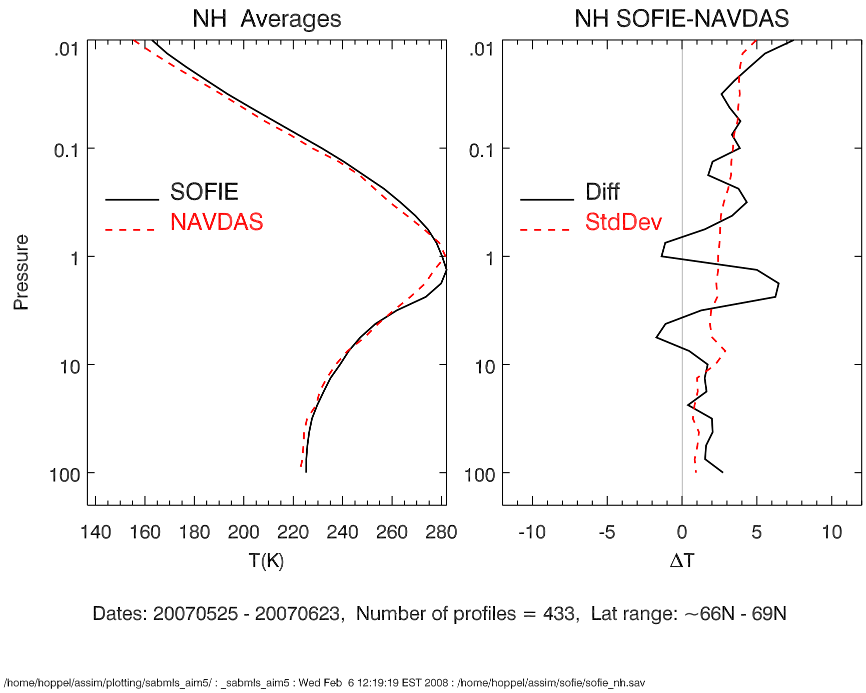

Fig. 6. (a) Mean temperatures from 25 May-23 June 2007 between 66°–69°N from 433 retrieved SOFIE profiles (black) and the NOGAPS-ALPHA analysis at the closest longitude, latitude and time to the SOFIE measurement (red); (b) corresponding mean bias (black) and standard deviation (red) between the two.

products.

Figure 6a compares the mean SOFIE temperatures from the northern hemisphere between 66°–69°N from 25 May to 23 June with analyzed temperature profiles from NOGAPS-ALPHA at the nearest longitude, latitude and time of each measurement (433 profiles in all). The comparisons reveal that SOFIE temperatures are already very close to the MLS and bias-corrected SABER temperatures assimilated by NOGAPS-ALPHA from 100-0.01 hPa. Figure 6b plots the corresponding mean bias and standard deviation, which are both generally small and increase slowly with altitude. The bias increases with height may be due to small errors in the SOFIE retrieval, while standard deviation increases with height may be related to small-scale noise in the NOGAPS-

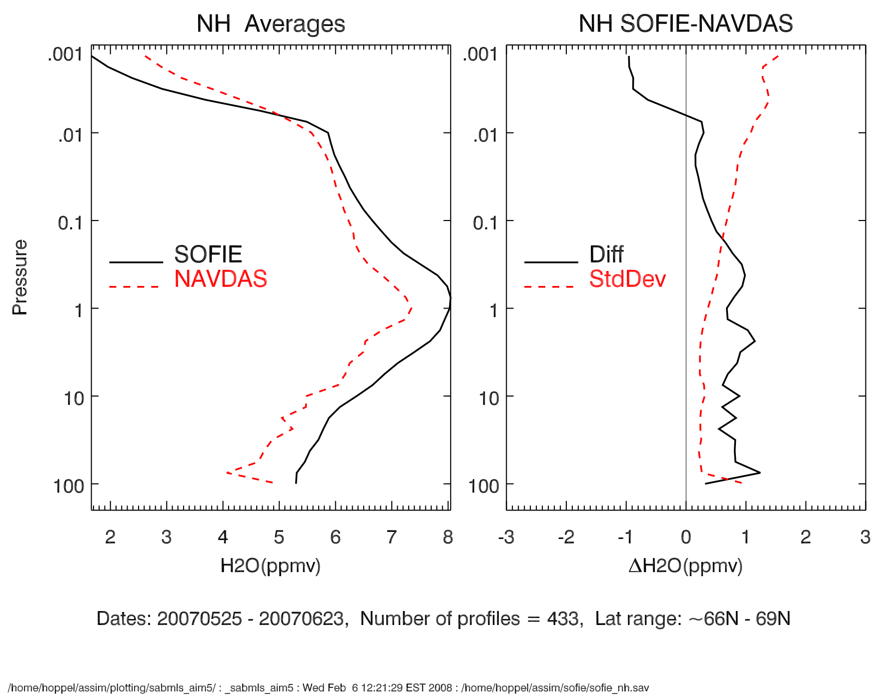

Fig. 7. Same presentation as in Figure 6 but for χ_{H_2O} (in ppmv).

ALPHA forecasts.

Figure 7 shows the corresponding plot for χ_{H_2O}, which reveals a systematic SOFIE wet bias throughout the stratosphere and lower mesosphere with respect to assimilated MLS water from NOGAPS-ALPHA. The high bias in these early experimental SOFIE χ_{H_2O} retrievals results from channel alignment biases caused by pressure registration and field-of-view offsets which are in the process of being corrected (Gordley, private communication, 2008). This comparison highlights the usefulness of NOGAPS-ALPHA as an early validation standard for emerging retrieval products from AIM instruments.

Finally we compare zonal-mean zonal winds, temperatures and ozone mixing ratios with lower-altitude DAS products from a more mature system: the NASA GEOS4 (Bloom et al., 2005). While the GEOS4 runs extend to 0.01 hPa, the standard analysis fields are issued only to 0.2 hPa as shown in Figure 8b. The overall June 2007 morphology of the mean zonal wind jets and

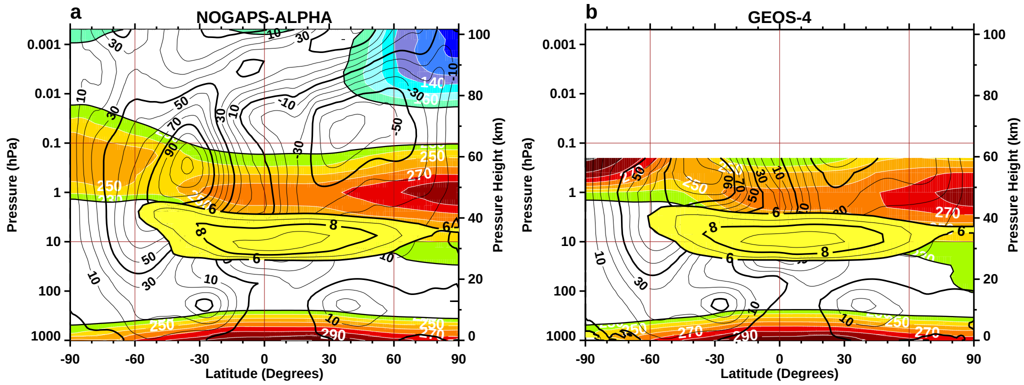

Fig. 8. Comparison of zonal-mean analysis output for June 2007 from (a) NOGAPS-ALPHA and (b) NASA GEOS4, showing zonal winds (m s^{-1}, black contours), temperatures (K, rainbow color scale and white contours), and ozone mixing ratios (ppmv, black contours in foreground yellow).

stratopause temperature structure is very similar in both analyses, apart from temperature differences near the polar winter stratopause. While the GWD parameter settings in NOGAPS-ALPHA may yield forecast biases in the winter hemisphere (see section 3), the NOGAPS-ALPHA polar winter stratopause temperatures compare better to MLS than the GEOS4 values (note that the TIMED satellite's yaw cycle had SABER preferentially viewing high northern latitudes at this time: see Figure 5). The zonal-mean peak ozone mixing ratios near 10 hPa are also very similar between the two analyses. The NOGAPS-ALPHA results at higher altitudes in Figure 8a show closure of the extratropical mesospheric zonal wind jets in both hemispheres and a cold mean polar summer mesopause. We now look in more detail at the polar summer MLT as described by the NOGAPS-ALPHA analysis fields.

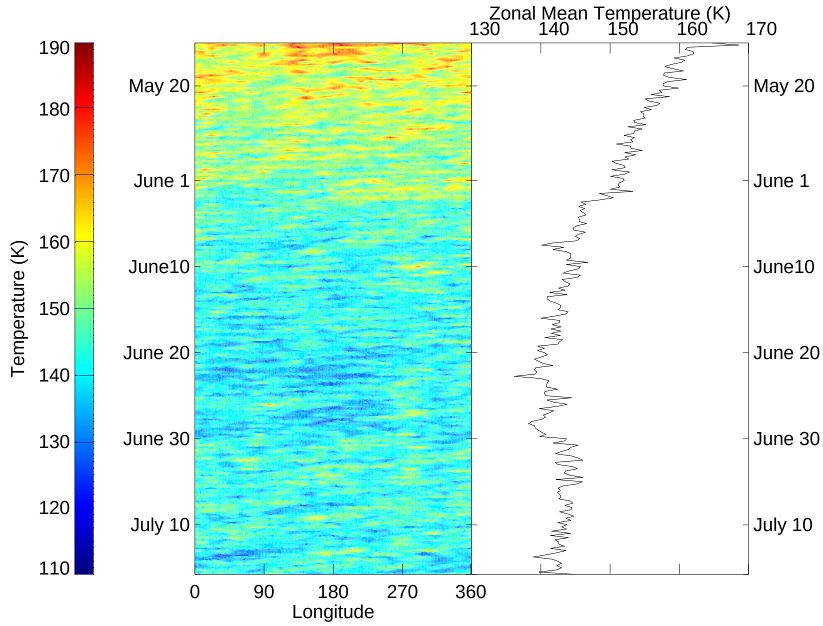

Fig. 9. Plot of mean temperatures between 65°–70°N at 0.006 hPa from 15 May-15 July 2007, shown in Hovmöller form on the left and the corresponding zonal-mean temperature time series on the right.

5 Mean Variations During PMC Season

Next we look at the mean polar summer MLT thermal conditions relevant to PMCs as provided from the analysis fields.

Figure 9 plots the time variation of temperature at 0.006 hPa (a typical PMC altitude) averaged between 65°–70°N. The analysis captures a gradual march to lower temperatures through May and June, yielding cold values in late June and mid July. The Hovmöller and zonal-mean plots both show spatial variability and temporal intermittency on both large and small scales throughout the season. Some of this can immediately be seen to be geophysical. For example, in late July a wavenumber-1 oscillation with a period of ~5 days is evident. Quasi 5-day waves in temperatures and other analyzed parameters are studied in greater depth in section 6.

Next we combine NOGAPS-ALPHA temperatures T and water vapor mixing ratios χ_{H_2O} to derive diagnostic saturation ratios for ice,

$$S = \frac{p_{H_2O}}{p_{ice}}, \tag{8}$$

at PMC altitudes, as follows. At a given analysis pressure p, the partial pressure of water vapor $p_{H_2O} = p\ \chi_{H_2O}$. We specify the saturation vapor pressure for ice, p_{ice}, using the Murphy and Koop (2005) fit

$$\log p_{ice} = 9.550426 - \frac{5723.265}{T} + 3.53068 \log T - 0.00728332\ T, \tag{9}$$

which is valid for T $\geq$110 K, and thus valid for PMC studies (Rapp and Thomas, 2006).

We have computed these diagnostic S values at PMC altitudes and compared them with the various indicators of cloud occurrence frequency derived from SOFIE data that are discussed by Stevens et al. (2008). One such comparison is summarized in Figure 10, which plots time series of zonal-mean diurnally-averaged NOGAPS-ALPHA saturation ratios S at 0.006 hPa in the 65°-70°N band. The dashed curve shows corresponding time series in this latitude band of PMC occurrence frequency derived from SOFIE data, taken from Figure 5 of Stevens et al. (2008). Except for the two large saturation spikes in the NOGAPS-ALPHA record, the overall agreement between the two time series is excellent, with an overall linear correlation coefficient of 0.78. Particularly noteworthy is the decrease in SOFIE PMC frequency around June 30, which is also seen in CIPS data (Merkel et al., this issue). This coincides with an abrupt $\sim$5 K increase in the zonal-mean temperature at 0.006 hPa at these

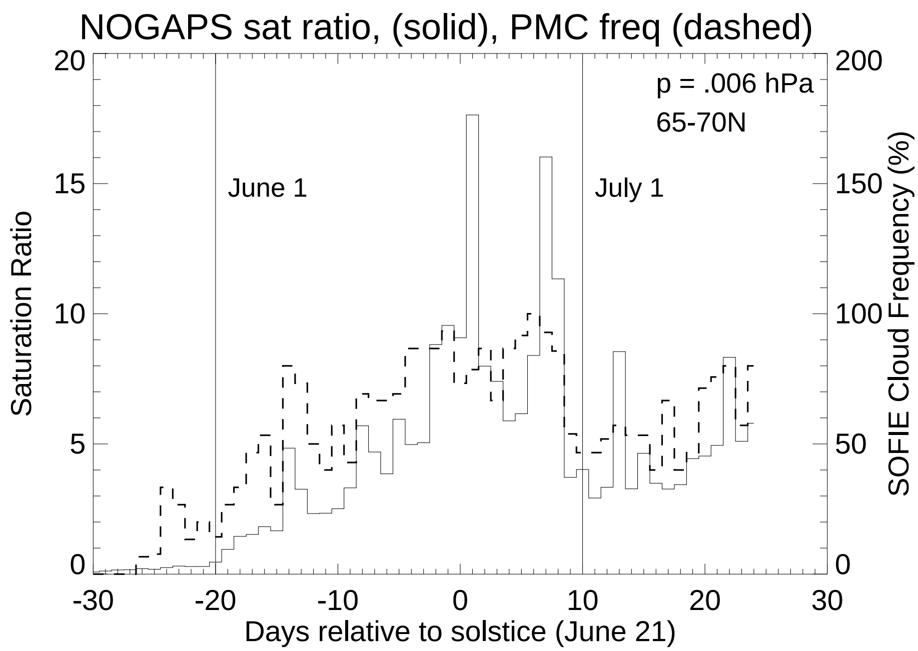

Fig. 10. NOGAPS-ALPHA saturation ratio S (solid curve, left hand axis) at 0.006 hPa between 65°–70°N compared with PMC occurrence frequency of bright clouds observed by SOFIE (dashed curve, right hand axis) taken from Figure 5 of Stevens et al. (2008). The linear correlation coefficient between the two curves is 0.78.

latitudes at the end of June, as seen in Figure 9.

6 Planetary Waves

As discussed in the introduction, accurate extraction of tides and fast planetary waves from asynoptic satellite data alone is difficult. Analysis systems like NOGAPS-ALPHA offer a potentially powerful tool for improving data-based planetary wave estimates, given that the forecast model ideally forecasts these waves and thus the DAS can optimally blend wave signals in both the observations y and a forecast background x_b constrained by analyzed initial conditions (Swinbank et al., 1999). Here we demonstrate the capability by per-

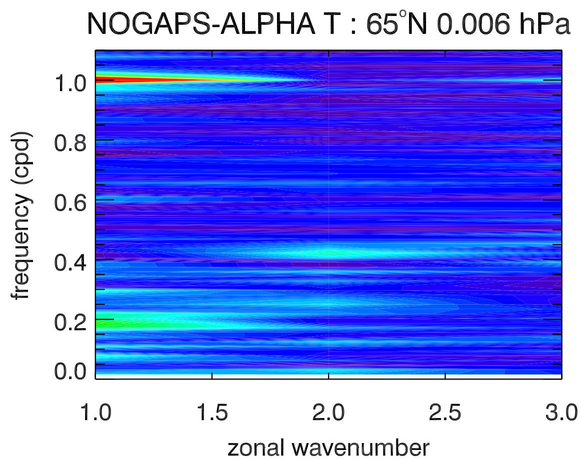

Fig. 11. Mean space-time magnitude of amplitude spectrum of temperature at 0.006 hPa and 65°N for westward propagating wavenumbers 1–3 over period 15 May to 18 July, 2007. Significant peaks (light blue, green and red) occur at wavenumber 1 at ∼5 days and 1 day, and at wavenumber 2 at ∼2 days. Color scale is linear.

forming space-time spectral analysis of the 6-hourly NOGAPS-ALPHA fields (Hayashi, 1982) at a range of altitudes to infer global amplitudes of particular planetary wave motions relevant to the polar summer MLT and PMCs (for further details on the algorithms used, see McCormack et al., 2008).

Figure 11 plots the mean space-time temperature spectrum of westward-propagating disturbances at 0.006 hPa and 65°N from 15 May 2007 to 18 July 2007. It shows peaks at wavenumber 1 at ∼ 5 days due to the westward-propagating (1,1) Rossby normal mode and at 1 day due to the migrating solar diurnal tide. We analyze these strong planetary wave signals in greater depth in what follows. Analysis of the ∼2 day wavenumber-2 Rossby normal mode (Merkel et al., 2008), which also appears (albeit more weakly) in Figure 11, is left for future studies.

6.1 *Quasi 5-Day Wave*

A number of studies have reported modulations in PMC occurrence by the quasi 5-day (1,1) Rossby normal mode (e.g., Kirkwood et al., 2002; Merkel et al., 2003; von Savigny et al., 2007; Merkel et al., 2008). Figure 12 shows mean values of peak temperature and meridional wind amplitude for June 2007, derived by scaling by $\sqrt{2}$ the RMS spectral power at westward-propagating wavenumber 1 over the 4.4-6.2 day period band. Inferred temperature amplitudes peak at midlatitudes and are weak at the equator, a latitudinal structure in broad agreement with previous modeling and observations of this mode (Hirota and Hirooka, 1984; Riggin et al., 2006). The peak amplitudes are generally weak with monthly-mean values in Figure 12a of $\sim$1–3 K in the summer MLT, in the range of previous observational estimates (e.g., von Savigny et al., 2007). Meridional wind responses, an indirect product of the assimilation, peak in Figure 12b primarily at the poles.

6.2 *Solar Migrating Tides*

Figure 13 plots peak amplitudes of the migrating diurnal tide averaged over the entire June 2007 analysis period, derived from spectral signals at westward-propagating wave-1 in a narrow frequency band centered at 1 day^{-1}. Figure 13a reveals an equatorial temperature peak of $\sim$5–10 K maximizing at lower altitudes slightly south of the equator, and a meridional wind peak of $\sim$25 m s^{-1} at $\sim$25°S latitude. Both results are in fairly good agreement with long-term data-validated CMAM results for June (Figure 2 of McLandress, 2002). Temperature amplitudes also agree well with amplitudes inferred from

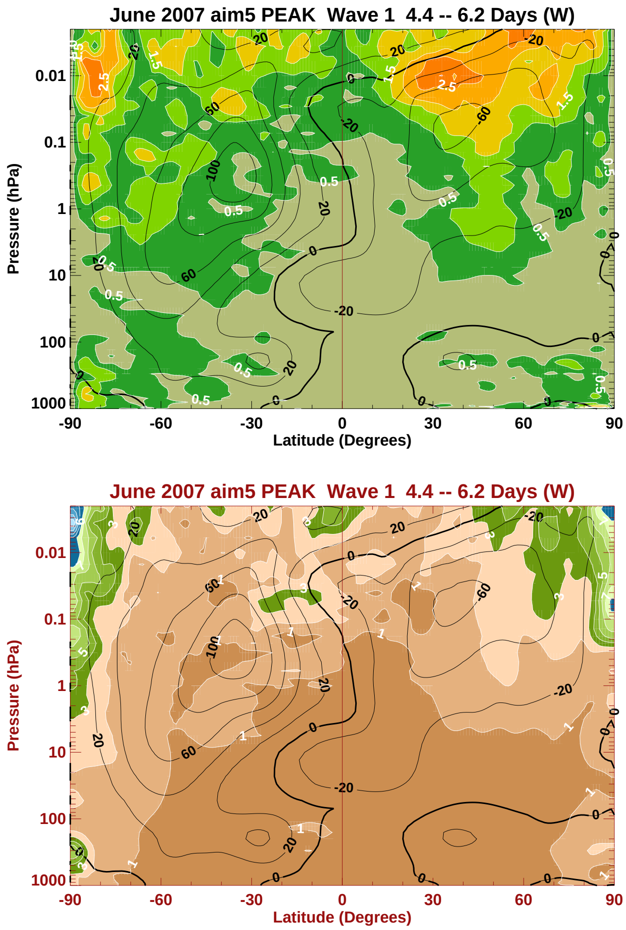

Fig. 12. White contours with associated color shading show peak amplitudes of the quasi 5-day wave computed over the 4.4-6.2 day period band from NOGAPS-ALPHA analyses for all of June 2007 in (a) temperature (Kelvin) and (b) merdional wind (m s^{-1}). Black contours on each panel show zonal-mean zonal winds (m s^{-1}) averaged over same period.

SABER temperatures during June 2004 by Zhang et al. (2006) and from UARS MLS temperatures by Forbes et al. (2006). At higher altitudes tidal peaks of $\sim$5 K also occur at extratropical summer MLT altitudes.

Figure 14 shows corresponding results for the migrating semidiurnal tide. Accurate assimilation of semidiurnal tides is particularly challenging, since they lie at the Nyquist period of our 6 hourly 3DVAR analysis window. Moreover,

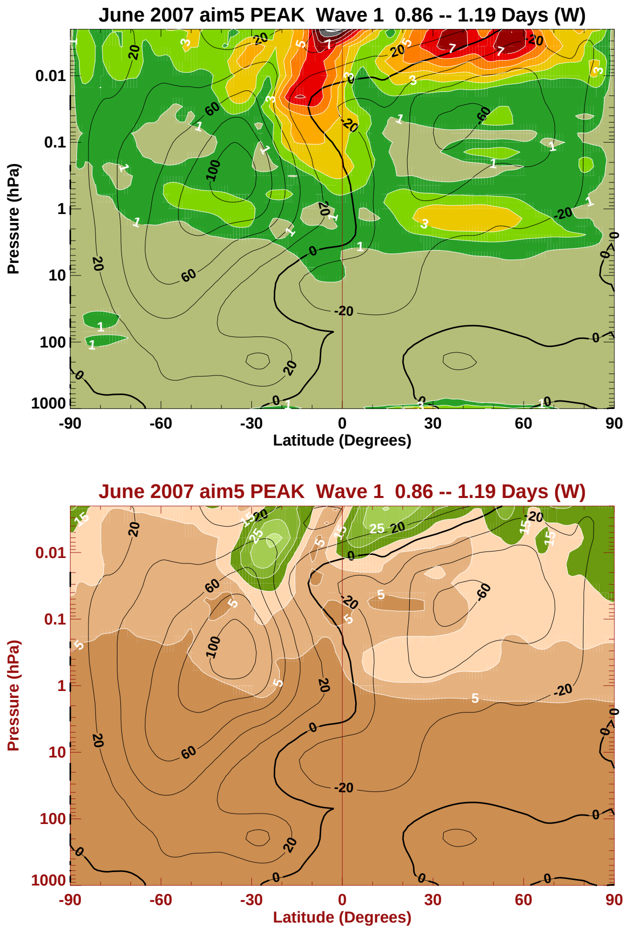

Fig. 13. White contours with associated color shading show peak diurnal tidal amplitudes from NOGAPS-ALPHA for all of June 2007 in (a) temperature (Kelvin) and (b) merdional wind (m s^{-1}). Black contours on each panel show zonal-mean zonal winds (m s^{-1}) averaged over same period.

the periodic quasi-diurnal variation in the 6-hourly longitudinal window for MLS and SABER data insertion essentially migrates with the Sun and may act as an artificial forcing term. Thus these semidiurnal results merit careful scrutiny.

Peak temperature amplitudes in Figure 14a show an extended high-altitude temperature peak at $\sim$40°S which agrees broadly with the predictions of tidal models (see Zhang et al., 2006). The June 2004 SABER results of Zhang et al. (2006) show a secondary peak nearer the equator, and our analyses show a number of similar secondary peaks at higher altitudes. In the summer MLT the temperature amplitudes are weaker in broad agreement with observations (e.g. Singer et al., 2003).

Our semidiurnal meridional-wind amplitudes in Figure 14b show two broad extratropical peaks peaking at $\pm$50–60° latitude of up to $\sim$20–30 m s^{-1}. Long-term radar measurements of winds in the Arctic MLT show climatological peak meridional wind amplitudes $\sim$10–20 m s^{-1} (Portnyagin et al., 2004). However, MLT winds measured by a meteor radar at Kühlungsborn (54°N) in June 2007 reveal stronger semidiurnal wind amplitudes of $\sim$20-30 m s^{-1} (see Figure 9 of Stevens et al., 2008) that appear to validate our indirectly inferred amplitudes of up to 25 m s^{-1} at this latitude in Figure 14b.

6.3 Planetary Wave Signals in Water Vapor

Figure 15 shows the quasi 5-day wave and diurnal tidal amplitude responses in NOGAPS-ALPHA assimilated water vapor fields. The 5-day wave amplitudes in Figure 15a show a broad peak in the summer MLT peaking at $\sim$60°–75°N. The peak amplitudes are $\sim$0.2-0.3 ppmv in the lower mesosphere. These findings are consistent with ground-based microwave water vapor data from ALOMAR (69°N) analyzed by Sonnemann et al. (2008), which show quasi 5-day oscillations of similar magnitude at a range of mesospheric altitudes in summer. They used a global model to explain these features in terms of 5-day wave-modulated horizontal transport across mean latitudinal water vapor gradients. Similarly located water vapor signals are seen for the diurnal tide in Figure 15b which, again, may indicate water vapor changes associated with

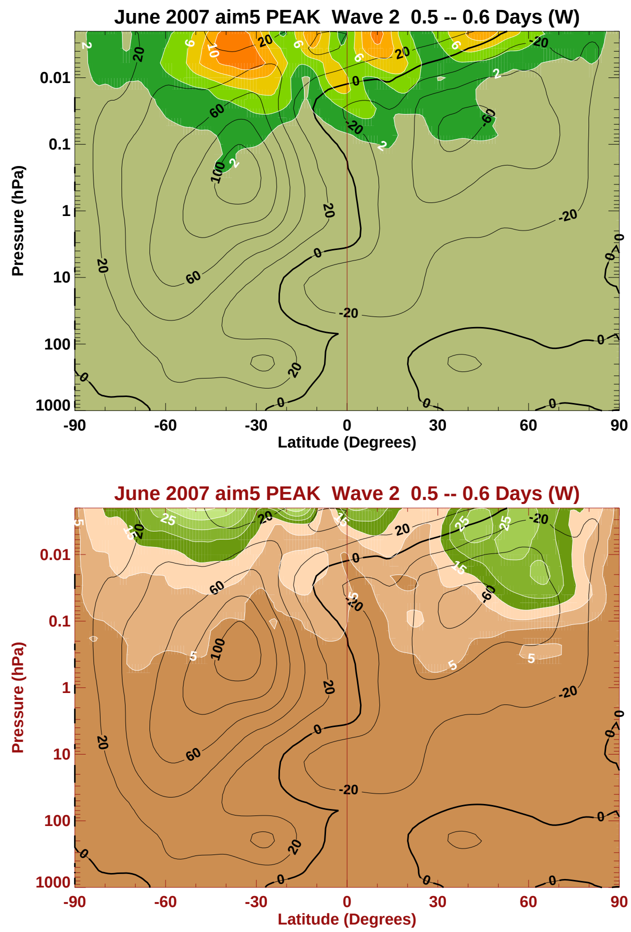

Fig. 14. As for Figure 13 but showing migrating semidiurnal tidal amplitudes.

diurnal tide-induced variations in meridional transport (e.g., Gerding et al., 2007).

In terms of PMCs, von Savigny et al. (2007) and Merkel et al. (2008) report strong anticorrelation between 5-day wave signals in temperature and PMC brightness. To investigate this for water vapor, Figure 16 plots the time evolution of the quasi 5-day wave amplitudes in NOGAPS-ALPHA temperature and water vapor at the 0.006 hPa level near nominal PMC altitudes. This was obtained by first performing a two-dimensional Fast Fourier Transform (2DFFT) of the fields, digitally filtering the spectral components to isolate westward zonal wavenumber 1 within the 4.4-6.25 day period band, performing

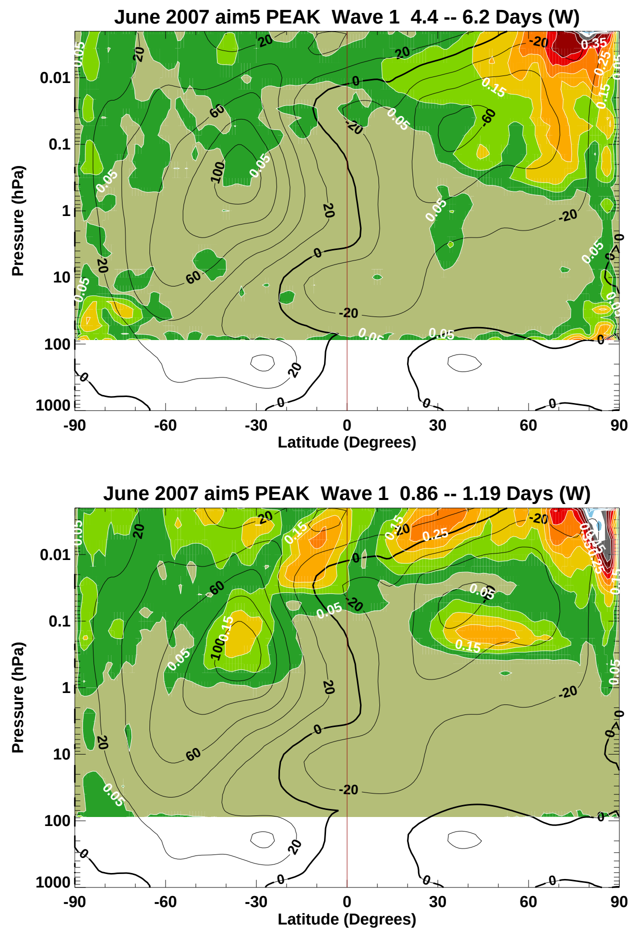

Fig. 15. White contours with associated color shading show peak amplitudes in water vapor (ppmv) for (a) quasi 5-day wave and (b) migrating diurnal tide for June 2007. Black contours on each panel show zonal-mean zonal winds (m s^{-1}) averaged over same period.

an inverse 2DFFT back to the space-time domain, then computing oscillation amplitude around a latitude circle at each latitude and time.

The temperature amplitudes in Figure 16a show considerable time variation, periodically intensifying then disappearing during May and June, and reaching largest amplitudes in early July. The corresponding water vapor amplitudes show a weak correlation with these temperature amplitude vacillations, and show largest amplitudes and greater day-to-day variability at polar latitudes

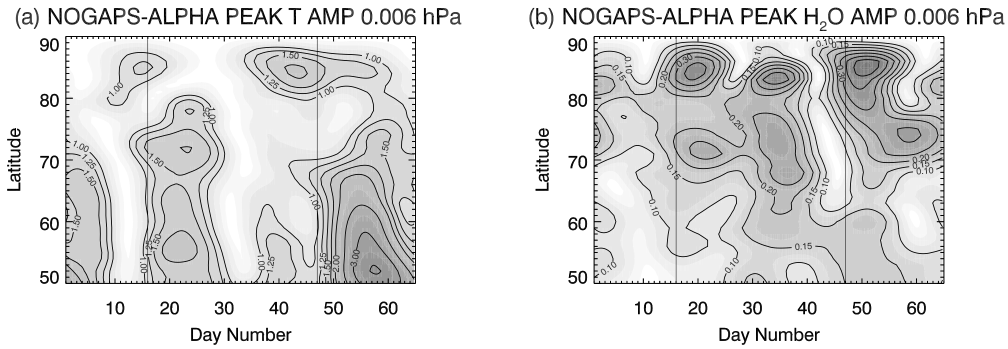

Fig. 16. Time series versus northern latitude of quasi 5-day wave peak amplitude at 0.006 hPa in (a) temperature (K), and (b) water vapor mixing ratio (ppmv). Time series starts on 15 May (day 1) and ends on 18 July (day 65). First day of June and July is marked with solid vertical line.

where 5-day wave meridional wind amplitudes peak (see Figure 12b). No obvious correlation between 5-day wave temperature and water vapor signals is evident in Figure 16, suggesting that the 5-day wave in water vapor mixing ratio near PMC altitudes is not as tightly coupled as the temperature and PMC-brightness responses at 5 days appear to be. Thus the 5-day wave signal in water vapor mixing ratios in Figure 16b may be a more complex net effect of temperature-modulated PMC microphysics, photolytic water vapor loss and horizontal transport across mean χ_{H_2O} gradients.

7 Sporadic Mid-Latitude Mesospheric Clouds

Equatorward of 50° latitude, mesospheric clouds (MCs) are considered by many as a novelty, where they are more popularly referred to as noctilucent clouds (NLCs: Taylor et al., 2002; Thomas et al., 2003). They are of global importance, however, because the transition region in an envionmental system is considered to be the most sensitive to change. Theoretical studies consistently indicate that climate trends should manifest themselves first in mid-latitude MCs (Thomas, 1996; Siskind et al., 2005).

The MC events that occur episodically at middle latitudes are not well understood (see, e.g., Herron et al., 2007). The global synoptic perspective afforded by NOGAPS-ALPHA assimilations is well suited to identification and analysis of such events. Here we illustrate the potential of NOGAPS-ALPHA fields to cast light on these mysterious events, leaving the deeper interpretation of the fundamental thermal and dynamical processes that seeded them for subsequent research.

7.1 MC event of 13 June 2007

The Spatial Heterodyne Imager of Mesospheric Radicals (SHIMMER) on STPSat-1 (Space Test Program Satellite-1) is a limb-viewing UV imager. The limb view geometry makes it well suited to detecting dimmer PMCs at lower latitudes since, unlike nadir sounders, the cloud signal does not need to be discriminated from a bright background.

Figure 17a plots all 236 UV limb profiles from 66–100 km altitude acquired by SHIMMER on 13 June 2007 between 40°–50°N. After removing the Rayleigh background using the technique described by Stevens et al. (2008), three profiles on this day, marked in red in Figure 17a, indicate presence of a mesospheric cloud at ∼80 km (Figure 17b).

The geographical locations of these three profiles are shown with red dots in Figure 18c. Successive panels plot maps of the NOGAPS-ALPHA temperature, water vapor mixing ratios and saturation ratios S at 0.006 hPa over the

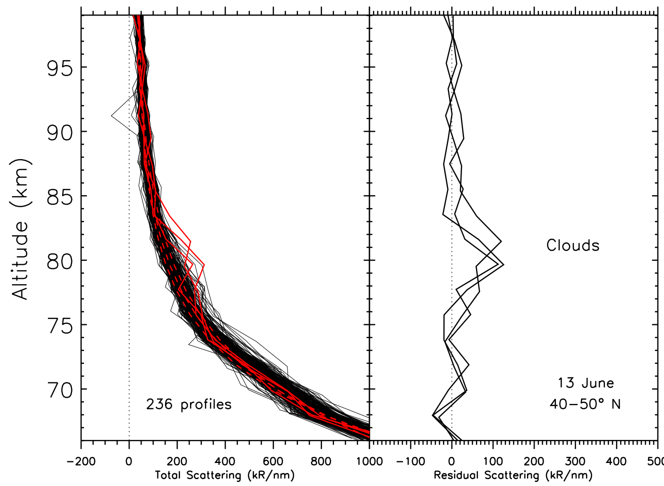

Fig. 17. SHIMMER mesospheric cloud detections on June 13, 2007. (a) All 236 limb brightness profiles taken between 40°–50°N on that day (black). The profiles are dominated by Rayleigh scattering. Scattering signal from mesospheric clouds is superimposed on this background contribution in three profiles plotted in red. (b) Difference between observed signals in (a) and fitted Rayleigh background for the three MC detections in (a).

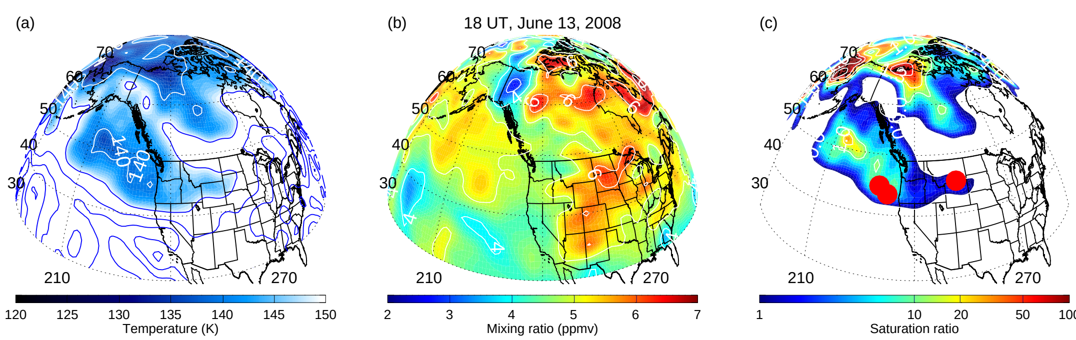

Fig. 18. Maps of analyzed NOGAPS-ALPHA (a) temperature (K), (b) water vapor mixing ratio (ppmv), and (c) saturation ratio S at 0.006 hPa on 13 June 2007 at 1800 UTC.

North American and Pacific regions on 13 June at 1800 UTC. These synoptic maps show an outbreak of cold mid-latitude MLT air below 150 K over the northern Pacific and northwestern US on this day. These low temperatures extend to nearly 40°N and yield saturation ratios in excess of unity across the northwestern US and northeastern Pacific regions where the 3 cloud events in Figure 17 were detected. These comparisons show that the diagnostic estimate of saturation ratio S based on analyzed NOGAPS-ALPHA temperature and water vapor fields shows skill in identifying this mid-latitude burst of MCs observed by SHIMMER. The maps indicate that mid-latitude mesospheric clouds can exist here at this time due to the cold supersaturated local environment, without the need in this case for additional local subgrid-scale gravity wave temperature cooling (e.g., Rapp et al., 2002) or rapid equatorward advection of cloud particles formed at cooler regions to the north (e.g., Gerding et al., 2007).

7.2 NLC Event of 19-20 June 2007

In the late evening hours of 19 June 2007 and into the morning of 20 June, spectacular displays of noctilucent clouds (NLCs) were widely reported and photographed by many amateur observers in Washington state and Oregon in the western United States[1], with bright NLCs photographed as far south as Bend, Oregon (44.0°N). The ground-based NLC observing network of Dalin et al. (2008) also reported very bright NLCs on this date at its western Canadian station.

Figure 19 plots the same sequence of temperature, water vapor and saturation ratios from the NOGAPS-ALPHA analysis of 20 June at 0600 UTC. The mesosphere over the northwestern US region is again cold, characterized by a tongue of cold air in Figure 19a that extends equatorward from polar regions

[1] see, e.g., `http://www.spaceweather.com/nlcs/gallery2007_page4.htm`

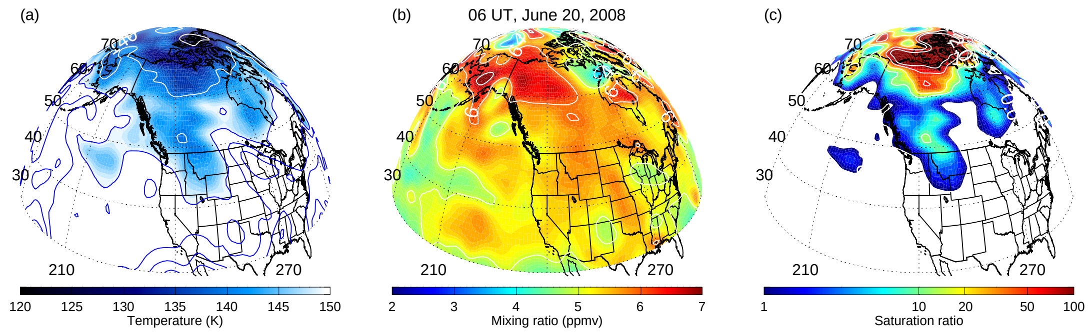

Fig. 19. Same presentation as Figure 18 but showing NOGAPS-ALPHA fields at 0.006 hPa on 20 June 2006 at 0600 UTC.

and within which moderate supersaturations occur in Figure 19c. Results on 1800 UTC (not shown) show this same feature has migrated westward to lie over the Pacific in a similar band of latitudes. The diagnostic S values from NOGAPS-ALPHA therefore appear consistent with these observed mid-latitude NLCs.

7.3 NLC Event of 30 June 2007

NLCs were reported and photographed on 29-30 June 2007 from many regions in Europe, including Sweden, Denmark, the United Kingdom, Hungary, and even as far south as Portugal[2].

The NOGAPS-ALPHA 0.006 hPa 0000 UTC analysis on 30 June 2007 in Figure 20 shows that an extensive pool of cold mesospheric air has moved over northwestern Europe. Particularly interesting in this event are collars of enhanced water vapor mixing ratios in Figure 20b that wrap equatorward from the eastern Atlantic and Eurasia into the United Kingdom and mid-latitude European countries. These water vapor enhancements combine with low tem-

[2] see, e.g., `http://www.spaceweather.com/nlcs/gallery2007_page6.htm`

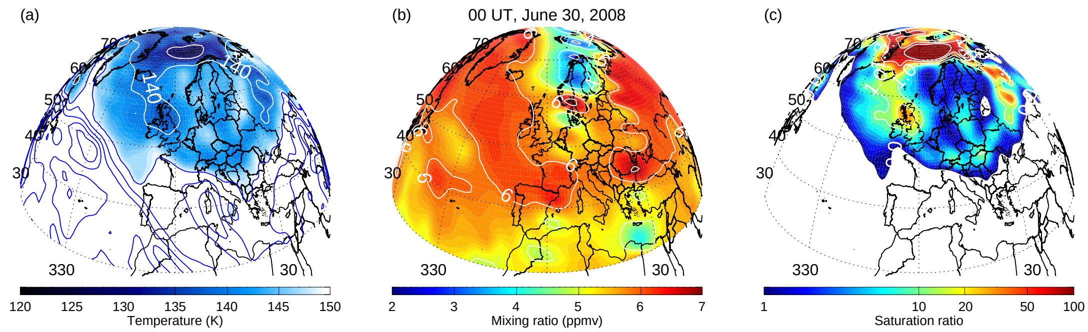

Fig. 20. Same presentation as Figure 18 but showing NOGAPS-ALPHA fields at 0.006 hPa on 30 June 2006 at 0000 UTC centered over western Europe.

peratures to yield large supersaturations in Figure 20c over, for example, the United Kingdom and Hungary. Again, the widespread reports of NLC displays over Europe at this time are borne out by enhanced mid-latitude saturation ratios in Figure 20c over broad swaths of the continent, as derived from analyzed NOGAPS-ALPHA temperature and water vapor fields.

8 Summary and Outlook

We have presented first results of a specific high-altitude assimilation of MLS and SABER temperatures and MLS water vapor and ozone mixing ratios using a new version of NOGAPS-ALPHA with a full DAS component extending to MLT altitudes. These experiments were carefully designed, tuned and performed during the northern summer MLT season from 15 May to 15 July, 2007, the first PMC season measured by instruments on the AIM satellite.

Assimilated temperatures from NOGAPS-ALPHA showed small biases with respect to SABER, MLS, SOFIE and GEOS4 temperatures at most altitudes and latitudes, including the polar summer MLT. Combining assimilated water vapor and temperature fields into saturation ratios S yielded excellent agreement with seasonal variations in SOFIE-based PMC frequency, as well as several separate mid-latitude MC/NLC events observed by SHIMMER and ground-based observers at various times in June 2007.

Spectral signatures of the quasi 5-day (1,1) Rossby normal mode and solar migrating diurnal and semidiurnal tides were isolated from the analyses and investigated as a function of height, latitude, time and assimilated parameter. The 5-day wave temperature amplitudes at PMC altitudes of $\sim$1–3 K were similar to those inferred in previous studies. A clear 5-day wave signal in water vapor mixing ratios in the polar summer MLT is also revealed, but which does not correlate directly with the 5-day wave in temperature. Diurnal and semidiurnal tidal amplitudes appeared to be broadly realistic, despite the intrinsic limitations of the 6-hourly 3DVAR data insertion process.

These preliminary results underscore how emerging ground-to-MLT global analysis fields provided by this and other NWP systems (e.g., Polavarapu et al., 2005a) offer new opportunities for MLT science. Within the specific context of AIM and PMCs, these fields can be used to systematically investigate some of the major scientific issues, such as: hemispheric asymmetries in summer polar MLT temperatures and PMC amount (Siskind et al., 2003); planetary wave modulation of PMCs (von Savigny et al., 2007); relative roles of vertical and horizontal transport on mid-latitude PMCs (Gerding et al., 2007), and; possible global teleconnections between PMCs in one hemisphere and polar stratospheric meteorological conditions in the other hemisphere (Karlsson et al., 2007). In helping to answer these and other specific questions, these MLT fields can begin to address deeper questions about the fundamental character of the MLT itself. For example, how predictable is the MLT (Hoppel et al., 2008)? Is MLT transport mainly local or nonlocal, and more specifically, is long-range horizontal transport in the MLT predictable or fundamentally chaotic (e.g., Holton and Schoeberl, 1988; Shepherd et al., 2000; Stevens et al., 2003)?

That having been said, current ground-to-MLT forecast-assimilation systems, including this one, are at the very early stages of their development and there is much left to do to improve them for future studies. In addition to assimilation of new data (e.g., SSMIS), new and improved model parameterizations and DAS algorithms are needed to handle the MLT region better (e.g., Polavarapu et al., 2005b; Sankey et al., 2007). Among the near-term foci for NOGAPS-ALPHA development are more completely tuned nonorographic GWD parameterizations for all latitudes and seasons, more complete diabatic heating and cooling rate parameterizations for the MLT, parameterizations of water vapor and ozone chemistry in the MLT, NNMI algorithms that work well in the MLT, better MLT bias correction schemes, and higher-altitude radiative forward models $\mathcal{H}$ for direct assimilation of MLT radiances into the system (Han et al., 2007). As the AIM mission continues through 2008, it will continue to offer a superb testbed environment for developing and validating these capabilities, which in turn should hopefully feed back to add value to AIM measurements and enhance the science return of this mission.

9 Acknowledgments

This research was supported by NASA, the Office of Naval Research, and the Defense Threat Reduction Agency. The NOGAPS-ALPHA runs were made possible by a grant of computer time from the DoD High Performance Computing Modernization Program at the Naval Oceanographic Office (NAVO) and Air Force Research Laboratory (AFRL) Major Shared Resource Centers. SHIMMER is a joint project between NRL and the DoD Space Test Program. We thank Victor Fomichev for his generous assistance with his radiative heating and cooling rate codes. Finally, we thank the AIM Science Team (principal investigator J. M. Russell III) for developing an outstanding mission.

References

Alexander M. J., Dunkerton, T. J., 1999. A spectral parameterization of mean flow forcing due to breaking gravity waves. Journal of the Atmospheric Sciences 56, 4167–4182.

Allen, D. R., Coy, L., Eckermann, S. D., McCormack, J. P., Manney, G. L., Hogan, T. F., Kim, Y.-J., 2006. NOGAPS-ALPHA simulations of the 2002 Southern Hemisphere stratospheric major warming. Monthly Weather Review 134, 498–518.

Arakawa, A., Suarez, M. J., 1983. Vertical differencing of the primitive equations in sigma coordinates. Monthly Weather Review 111, 34–45.

Azeem, S. M. I., Killeen, T. L., Johnson, R. M., Wu, Q., Gell, D. A., 2000. Space-time analysis of TIMED Doppler Interferometer (TIDI) measurements. Geophysical Research Letters 27, 3297–3300.

Baker, N. L., Hogan, T. F., Campbell, W. F., Pauley, R. L., Swadley, S. D., 2005. The impact of AMSU-A radiance assimilation in the U.S. Navy's Operational Global Atmospheric Prediction System (NOGAPS), Naval Research Laboratory Memorandum Report, NRL/MR/7530–05-8836, 22pp.

Baker, N. L., Goerss, J., Sashegyi, K., Pauley, P., Langland, R., Xu, L., Blankenship, C., Campbell, B., Ruston, B., Rosmond, T., Pauley, R. L.,

2007. An overview of the NRL Atmospheric Variational Data Assimilation (NAVDAS) and NAVDAS-AR (Accelerated Representer) systems, 18th. AMS Conference on Numerical Weather Prediction, 25-29 June, Park City, UT, Paper 2B.1, 6pp (available at `http://ams.confex.com/ams/pdfpapers/124031.pdf`).

Ballish, B., Cao, X., Kalnay, E., Kanamitsu, M., 1992. Incremental nonlinear normal-mode initialization. Monthly Weather Review 120, 1723–1734.

Becker, E., Fritts, D. C., 2006. Enhanced gravity-wave activity and interhemispheric coupling during the MaCWAVE/MIDAS northern summer program 2002. Annales Geophysicae 24, 1175–1188.

Berger, U., von Zahn, U., 2007. Three-dimensional modeling of the trajectories of visible noctilucent cloud particles: An indication of particle nucleation well below the mesopause. Journal of Geophysical Research 112, D16204, doi:10.1029/2006JD008106.

Bloom, S., da Silva, A., Dee, D., Bosilovich, M., Chern, J.-D., Pawson, S., Schubert, S., Sienkiewicz, M., Stajner, I., Tan, W.-W., Wu, M.-L., 2007. Documentation and validation of the Goddard Earth Observing System (GEOS) data assimilation system - version 4, NASA Tech. Mem. NASA/TM–2005–104606, 15, *Technical Report Series on Global Modeling and Data Assimilation*, M. J. Suarez ed., 165pp. [available online at `http://ntrs.nasa.gov`]

Burrage, M. D., Hagan, M. E., Skinner, W. R., Wu, D. L., Hays, P. B., 1995. Long-term variability in the solar diurnal tide observed by HRDI and simulated by the GSWM. Geophysical Research Letters 22, 2641–2644.

Charron, M., Manzini, E., 2002. Gravity waves from fronts: Parameterization and middle atmosphere response in a general circulation model. Journal of the Atmospheric Sciences 59, 923–941.

Chou, M.-D., Suarez, M. J., 1999. A solar radiation parameterization for atmospheric studies, NASA Technical Memorandum NASA/TM-1999-104606, volume 15, *Technical Report Series on Global Modeling and Data Assimilation*, edited by M. J. Suarez, 40 pp. (Available at `http://ntrs.nasa.gov`).

Chou, M.-D., Suarez, M. J., Liang, X.-Z. Liang, Yan M. M.-H., 2001. A thermal infrared radiation parameterization for atmospheric studies, NASA Technical Memorandum NASA/TM-2001-104606, volume 19, *Technical Report Series on Global Modeling and Data Assimilation*, edited by M. J. Suarez, 56 pp. (Available at `http://ntrs.nasa.gov`).

Coy, L., Allen, D. R., Eckermann, S. D., McCormack, J. P., Stajner, I., Hogan, T. F., 2007. Effects of model chemistry and data biases on stratospheric ozone assimilation. Atmospheric Chemistry and Physics 7, 2917–2935.

Daley, R., Barker, E., 2001a. NAVDAS: Formulation and diagnostics. Monthly Weather Review 129, 869–883.

Daley, R., Barker, E., 2001b. NAVDAS source book 2001. Naval Research Laboratory Publication NRL/PU/7530–01-441, 163pp.

Dalin, P., and coauthors, 2008. Ground-based observations of noctilucent clouds with an inter-continental network of automatic digital cameras. Journal of Atmospheric and Solar-Terrestrial Physics (in press).

Dee, D., daSilva, A. M., 1998. Data assimilation in the presence of forecast bias. Quarterly Journal of the Royal Meteorological Society 124, 269–295.

Drob, D. P., Picone, J. M., Eckermann, S. D., She, C. Y., Kafkalidis, J. F., Ortland, D. A., Niciejewski, R. J., Killeen, T. L., 2000. Mid-latitude temperatures at 87 km: Results from multi-instrument Fourier analysis. Geophysical Research Letters 27, 2109–2112.

Eckermann, S. D., 2008. Hybrid σ–p coordinate choices for a global model.

Monthly Weather Review (submitted).

Eckermann, S. D., McCormack, J. P., Coy, L., Allen, D., Hogan, T., Kim, Y.-J., 2004. NOGAPS-ALPHA: A prototype high altitude global NWP model, Preprint Volume of the Symposium on the 50th. Anniversary of Operational Numerical Weather Prediction, American Meteorological Society, University of Maryland, College Park, MD, 1417 June 2004, Paper P2.6, 23pp (available online at http://uap-www.nrl.navy.mil/dynamics/papers/EckermannP2.6-reprint.pdf).

Eckermann, S. D., Broutman, D., Stollberg, M. T., Ma, J., McCormack, J. P., Hogan, T. F., 2007. Atmospheric effects of the total solar eclipse of 4 December 2002 simulated with a high-altitude global model. Journal of Geophysical Research 112, D14105, doi:10.1029/2006JD007880.

Fomichev, V. I., Blanchet, J.-P., Turner, D. S., 1998. Matrix parameterization of the 15 μm CO_2 band cooling in the middle and upper atmosphere for variable CO_2 concentration. Journal of Geophysical Research 103, 11,505–11,528.

Fomichev, V. I., Ogibalov, V. P., Beagley, S. R., 2004. Solar heating by the near-IR CO_2 bands in the mesosphere. Geophysical Research Letters 31, L21102, doi:10.1029/2004GL020324.

Forbes, J. M., Kilpatrick, M., Fritts, D., Manson, A. H., Vincent, R. A., 1997. Zonal mean and tidal dynamics from space: An empirical examination of aliasing and sampling issues. Annales Geophysicae 15, 1158–1164.

Forbes, J. M., Wu, D., Zhang, X., 2006. Solar tides as revealed by measurements of mesosphere temperature by the MLS experiment on UARS, Journal of the Atmospsheric Sciences 63, 1776–1797.

Fritts, D. C., Luo, Z., 1995. Dynamical and radiative forcing of the summer mesopause and thermal structure, 1, mean soltice conditions. Journal of

Geophysical Research 100, 3119–3128.

Garcia, R. R., Marsh, D. R., Kinnison, D. E., Boville, B. A., Sassi, F., 2007. Simulation of secular trends in the middle atmosphere, 1950–2003. Journal of Geophysical Research 112, D09301, doi:10.1029/2006JD007485.

Geer, A. J., Lahoz, W. A., Jackson, D. R., Cariolle, D., McCormack J. P., 2007. Evaluation of linear ozone photochemistry parametrizations in a stratosphere-troposphere data assimilation system. Atmospheric Chemistry and Physics 7, 939–959.

Gerding, M., Höffner, J., Rauthe, M., Singer, W., Zecha, M., Lübken, F.-J., 2007. Simultaneous observation of noctilucent clouds, mesospheric summer echoes, and temperature at a midlatitude station (54°N). Journal of Geophysical Research 112, D12111, doi:10.1029/2006JD008135.

Gordley, L. L., and coauthors, 2008. The Solar Occultation for Ice Experiment. Journal of Atmospheric and Solar Terrestrial Physics (this issue).

Hamilton, K., 1997. The role of parameterized drag in a troposphere-stratosphere-mesosphere general circulation model. *Gravity Wave Processes - Their Parameterization in Global Climate Models*, NATO ASI Series, Vol. I 50, K. Hamilton ed., Springer-Verlag, Berlin Heidelberg, 337–350.

Han, Y., Weng, F., Liu, Q., van Delst, P., 2007. A fast radiative transfer model for SSMIS upper atmosphere sounding channels. Journal of Geophysical Research 112, D11121, doi:10.1029/2006JD008208.

Harshvardhan, Davies, R., Randall, D., Corsetti, T., 1987. A fast radiation parameterization for atmospheric circulation models. Journal of Geophysical Research 92, 1009–1016.

Hayashi, Y., 1982. Space-time spectral analysis and its applications to atmospheric waves. Journal of the Meteorological Society of Japan 60, 156–171.

Herron, J. P., Wickwar, V. B., Espy, P. J., Meriwether, J. W., 2007. Observations of a noctilucent cloud above Logan, Utah (41.7°N, 118.8°W) in 1995. Journal of Geophysical Research 112, D19203, doi:10.1029/2006JD007158.

Hirota, I., Hirooka, T., 1984. Normal mode Rossby waves observed in the upper stratosphere, part 1: first symmetric modes of zonal wavenumbers 1 and 2. Journal of the Atmospheric Sciences 41, 1253–1267.

Hogan, T. F., 2007. Land surface modeling in the Navy Operational Global Atmospheric Prediction System, Paper 11B.1, Preprint Volime of 22nd. AMS Conference on Weather Analysis and Forecasting/18th. Conference on Numerical Weather Prediction, Park City, UT (available online at http://ams.confex.com/ams/22WAF18NWP/techprogram/paper_123403.htm)

Hogan, T. F., Rosmond, T. E., 1991. The description of the Navy Operational Global Atmospheric Prediction System's spectral forecast model. Monthly Weather Review 119, 1786–1815.

Hogan, T. F., Rosmond, T. E., Gelaro, R., 1991. The NOGAPS forecast model: a technical description, Naval Oceanographic and Atmospheric Research Laboratory Report No. 13, 219pp.

Holton, J. R., Schoeberl, M. R., 1988. The role of gravity wave generated advection and diffusion in transport of tracers in the mesosphere, Journal of Geophysical Research 93, 11,075–11,082.

Hoppel, K. W., Baker, N. L., Coy, L., Eckermann, S. D., McCormack, J. P., Nedoluha, G., Siskind, D. E., 2008. Assimilation of stratospheric and mesospheric temperatures from MLS and SABER in a global NWP model. Atmospheric Chemistry and Physics Discussions (in press).

Jiang, Y. B., and coauthors, 2007. Validation of Aura Microwave Limb Sounder ozone by ozonesonde and lidar measurements. Journal of Geophysical Research 112, D24S34, doi:10.1029/2007JD008776.

Karlsson, B., Körnich, H., Gumbel, J., 2007. Evidence for interhemispheric stratosphere-mesosphere coupling derived from noctilucent cloud properties. Geophysical Research Letters 34, L16806, doi:10.1029/2007GL030282.

Kerola, D. X., 2006. Calibration of Special Sensor Microwave Imager/Sounder (SSMIS) upper air brightness temperature measurements using a comprehensive radiative transfer model. Radio Science 41, RS4001, doi:10.1029/2005RS003329.

Kirkwood, S., and coauthors, 2002. Noctilucent clouds, PMSE, and 5-day planetary waves: a case study. Geophysical Research Letters 29(10), 1411, doi:10.1029/2001GL014022.

Kutepov, A. A., Feofilov, A. G., Marshall, B. T., Gordley, L. L., Pesnell, W. D., Goldberg, R. A., Russell III, J. M., 2006. SABER temperature observations in the summer polar mesosphere and lower thermosphere: Importance of accounting for the CO_2 ν_2 quanta V–V exchange. Geophysical Research Letters 33, L21809, doi:10.1029/2006GL026591.

Lambert, A., and coauthors, 2007. Validation of the Aura Microwave Limb Sounder middle atmosphere water vapor and nitrous oxide measurements. Journal of Geophysical Research 112, D24S36, doi:10.1029/2007JD008724.

Lindzen, R. S., 1981. Turbulence and stress due to gravity wave and tidal breakdown. Journal of Geophysical Research 86, 9701–9714.

Lipton, A. E., 2002. Polarization of measurement for microwave temperature sounding of the mesosphere. IEEE Transactions on Geoscience and Remote Sensing 40, 1669–1681.

Louis, J. F., 1979. A parametric model of vertical eddy fluxes in the atmosphere, Boundary Layer Meteorolology 17, 187–202.

Louis, J. F., Tiedtke, M., and Geleyn, J. F., 1982. A short history of the operational PBL parameterization at ECMWF, ECMWF Workshop on Planetary

Boundary Parameterizations, 25-27 November 1981, 59–79.

Manney, G. L., and coauthors, 2007. Solar occultation satellite data and derived meteorological products: Sampling issues and comparisons with Aura Microwave Limb Sounder. Journal of Geophysical Research 112, D24S50, doi:10.1029/2007JD008709.

Marsh, D. R., Skinner, W. R., Marshall, A. R., Hays, P. B., Ortland, D. A., Yee, J.-H., 2002. High Resolution Doppler Imager observations of ozone in the mesosphere and lower thermosphere. Journal of Geophysical Research 107(D19), 4390, doi:10.1029/2001JD001505.

McCormack, J. P., Eckermann, S. D., Coy, L., Allen, D. R., Kim, Y.–J., Hogan, T., Lawrence, B. N., Stephens, A., Browell, E. V., Burris, J., McGee, T., Trepte, C. R., 2004. NOGAPS-ALPHA model simulations of stratospheric ozone during the SOLVE2 campaign. Atmospheric Chemistry and Physics 4, 2401–2423.

McCormack, J. P., Eckermann, S. D., Siskind, D. E., McGee, T. J., 2006. CHEM2D-OPP: A new linearized gas-phase ozone photochemistry parameterization for high-altitude NWP and climate models. Atmospheric Chemistry and Physics 6, 4943–4972.

McCormack, J. P., Hoppel, K. W., Eckermann, S. D., Coy, L., Siskind, D. E., 2008. NOGAPS-ALPHA simulations of the quasi-two day wave in mesospheric temperature and water vapor during January 2006. Atmospheric Chemistry and Physics Discussions (in preparation).

McLandress, C., 1998. On the importance of gravity waves in the middle atmosphere and their parameterization in general circulation models. Journal of Atmospheric and Solar-Terrestrial Physics 60, 1357–1383.

McLandress, C., 2002. The seasonal variation of the propagating diurnal tide in the mesosphere and lower thermosphere. Part I: The role of gravity waves and planetary waves. Journal of the Atmospheric Sciences 59, 893–906.

McLandress, C., Zhang, S. P., 2007. Satellite observations of mean winds and tides in the lower thermosphere: 1. Aliasing and sampling issues. Journal of Geophysical Research 112, D21104, doi:10.1029/2007JD008456.

McClintock, W. E., and coauthors, 2008. The Cloud Imaging and Particle Size (CIPS) experiment on the Aeronomy of Ice in the Mesosphere (AIM) spacecraft. Journal of Atmospheric and Solar Terrestrial Physics (this issue).

Merkel, A. W., Thomas, G. E., Palo, S. E., Bailey, S. M., 2003. Observations of the 5-day planetary wave in PMC measurements from the Student Nitric Oxide Explorer satellite. Geophysical Research Letters 30(4), doi:10.1029/2002GL016524.

Merkel, A. W., Garcia, R. R., Bailey, S. M., Russell III, J. M., 2008. Observational studies of planetary waves in PMCs and mesospheric temperatures measured by SNOE and SABER. Journal of Geophysical Research (in press).

Mertens, C. J., and coauthors, 2004. SABER observations of mesospheric temperatures and comparisons with falling sphere measurements taken during the 2002 summer MaCWAVE campaign. Geophysical Research Letters 31, L03105, doi:10.1029/2003GL018605.

Murphy, D. M., Koop, T., 2005. Review of the vapour pressures of ice and supercooled water for atmospheric applications. Quarterly Journal of the Royal Meteorological Society 131, 1539–1565.

Norton, W. A., Thuburn, J., 1999. Sensitivity of mesospheric mean flow, planetary waves, and tides to strength of gravity wave drag. Journal of Geophysical Research 104(D24), 30897–30912, 10.1029/1999JD900961.

Oberheide, J., Hagan, M. E., Roble R. G., 2003. Tidal signatures and aliasing in temperature data from slowly precessing satellites. Journal of Geophysical

Research 108(A2), 1055, doi:10.1029/2002JA009585.

Palmer, T. N., Shutts, G. J., Swinbank, R., 1986. Allevation of a systematic westerly bias in general circulation and numerical weather prediction models through an orographic gravity wave drag parameterization. Quarterly Journal of the Royal Meteorological Society 112, 1001–1039.

Peng, M. S., Ridout, J. A., Hogan, T. F., 2004. Recent modifications of the Emanuel convective scheme in the Navy Operational Global Atmospheric Prediction System. Monthly Weather Review 132, 1254–1268.

Polavarapu, S., Ren, S., Rochon, Y., Sankey, D., Ek, N., Koshyk, J., Tarasick, D., 2005a. Data assimilation with the Canadian middle atmosphere model. Atmosphere-Ocean 43, 77–100.

Polavarapu, S., Shepherd, T. S., Rochon, Y., Ren, S., 2005b. Some challenges of middle atmosphere data assimilation. Quarterly Journal of the Royal Meteorological Society 131, 3513–3527.

Portnyagin, Y. I., and coauthors, 2004. Monthly mean climatology of the prevailing winds and tides in the Arctic mesosphere/lower thermosphere. Annales Geophysicae 22, 3395–3410.

Rapp, M., Thomas, G. E., 2006. Modeling the microphysics of mesospheric ice particles: Assessment of current capabilities and basic sensitivities. Journal of Atmospheric and Solar–Terrestrial Physics 68, 715–744.

Rapp, M., Lübken, F.-J., Müllemann, A., Thomas, G. E., Jensen, E. J., 2002. Small-scale temperature variations in the vicinity of NLC: Experimental and model results. Journal of Geophysical Research 107(D19), 4392, doi:10.1029/2001JD001241.

Read, W. G., and coauthors, 2007. Aura Microwave Limb Sounder upper tropospheric and lower stratospheric H_2O and relative humidity with respect to ice validation. Journal of Geophysical Research 112, D24S35, doi:10.1029/2007JD008752.

Riggin, D. M., and coauthors, 2006. Observations of the 5-day wave in the mesosphere and lower thermosphere. Journal of Atmospheric and Solar-Terrestrial Physics 68, 323–339.

Russell III, J. M., and coauthors, 2008. Aeronomy of Ice in the Mesosphere (AIM): A satellite mission to study polar mesospheric clouds. IEEE Transactions on Geoscience & Remote Sensing (in press).

Sankey, D., Ren, S., Polavarapu, S., Rochon, Y. J., Nezlin, Y., Beagley, S., 2007. Impact of data assimilation filtering methods on the mesosphere. Journal of Geophysical Research 112, D24104, doi:10.1029/2007JD008885.

Sassi, F., Boville, B. A., Kinnison, D., Garcia, R. R., 2005. The effects of interactive ozone chemistry on simulations of the middle atmosphere. Geophysical Research Letters 32, L07811, doi:10.1029/2004GL022131.

Schwartz, M. J., and coauthors, 2008. Validation of the Aura Microwave Limb Sounder temperature and geopotential height measurements. Journal of Geophysical Resarch, doi:10.1029/2007JD008783, in press.

Seaman, R. S., Bourke, W. P. Bourke, Steinle, P., Hart, T., Embery, G., Naughton, M., Rikus, L., 1995. Evolution of the Bureau of Meteorology's global assimilation and prediction system. part 1: Analysis and initialization. Australian Meteorological Magazine 44, 1–18.

Shaw, T. A., Shepherd, T. G., 2007. Angular momentum conservation and gravity wave drag parameterization: Implications for climate models. Journal of the Atmospheric Sciences 64, 190–203.

Shepherd, T. G., Koshyk, J. N., Ngan, K., 2000. On the nature of large-scale mixing in the stratosphere and mesosphere. Journal of Geophysical Research 105, 12,433–12,446.

Simmons, A. J., Burridge, D. M., 1981. An energy and angular momentum conserving vertical finite-difference scheme and hybrid vertical coordinates. Monthly Weather Review 109, 758–766.

Singer, W., Bremer, J., Hocking, W. K., Weiss, J., Latteck, R., Zecha, M., 2003. Temperature and wind tides around the summer mesopause at middle and Arctic latitudes. Advances in Space Research 31(9), 2055–2060.

Siskind, D. E., Eckermann, S. D., McCormack, J. P., Alexander, M. J., Bacmeister, J. T., 2003. Hemispheric differences in the temperature of the summertime stratosphere and mesosphere. Journal of Geophysical Research 108(D2), 4051, doi:10.1029/2002JD002095.

Siskind, D. E., Stevens, M. H., Englert, C. R., 2005. A model study of global variability in mesospheric cloudiness. Journal of Atmospsheric and Solar-Terrestrial Physics 67, 501–513.

Siskind D. E., Eckermann, S. D., Coy, L, McCormack, J. P., Randall, C. E., 2007. On recent interannual variability of the Arctic winter mesosphere: Implications for tracer descent. Geophysical Research Letters 34, L09806, doi:10.1029/2007GL029293.

Slingo, J. M., 1987. The development and verification of a cloud prediction scheme in the ECMWF model. Quarterly Journal of the Royal Meteorological Society 113, 899–927.

Sonnemann, G. R., Hartogh, P., Grygalashvyly, M., Song, L., Berger, U., 2008. The quasi 5-day signal in the mesospheric water vapor concentration at high latitudes in 2003 – a comparison between observations at ALOMAR and calculations. Journal of Geophysical Research (in press).

Stevens, M. H., Gumbel, J., Englert, C. R., Grossmann, K. U., Rapp, M., Hartogh, P., 2003. Polar mesospheric clouds formed from space shuttle exhaust. Geophysical Research Letters 30(10), 1546, doi:10.1029/2003GL017249.

Stevens, M. H., Englert, C. R., Hervig, M., Petelina, S. V., Singer, W., Nielsen, K., 2008. The diurnal variation of noctilucent cloud frequency near 55°N observed by SHIMMER. Journal of Atmospheric and Solar-Terrestrial Physics (this issue).

Susskind, J., Barnet, C., Blaisdell, J., Iredell, L., Keita, F., Kouvaris, L., Molnar, G., Chahine, M., 2006. Accuracy of geophysical parameters derived from Atmospheric Infrared Sounder/Advanced Microwave Sounding Unit as a function of fractional cloud cover. Journal of Geophysical Research 111, D09S17, doi:10.1029/2005JD006272.

Swinbank, R., Orris, R. L., Wu, D. L., 1999. Stratospheric tides and data assimilation. Journal of Geophysical Research 104, 16,929–16,942.

Taylor, M. J., Gadsden, M., Lowe, R. P., Zalcik, M. S., Brausch, J., 2002. Mesospheric cloud observations at unusually low latitudes, Journal of Atmospheric and Solar-Terrestrial Physics 64, 991–999.

Teixeira, J., Hogan, T., 2002. Boundary layer clouds in a global atmospheric model: Simple cloud cover parameterization. Journal of Climate 15, 1261–1276.

Thomas, G. E., 1996. Is the polar mesosphere the miners canary of global change? Advances in Space Research 18, 149–158.

Thomas, G.E. and coauthors, 2003. Comment on “Are noctilucent clouds truly a “Miners Canary” for global change”, Eos 84(36), 352–353.

Tiedtke, M., 1984. The sensitivity of the time-scale flow to cumulus convection in the ECMWF model, Workshop on Large-Scale Numerical Models, 28 November - 1 December 1983, ECMWF, 297–316.

Trenberth, K. E., Stepaniak, D. P., 2002. A pathological problem with NCEP reanalyses in the stratosphere, Journal of Climate 15, 690–695.

von Savigny, C., Robert, C., Bovensmann, H., Burrows, J. P., Schwartz, 2007. Satellite observations of the quasi 5-day wave in noctilucent clouds and mesopause temperatures. Geophysical Research Letters 34, L24808, doi:10.1029/2007GL030987.

Webster, S., Brown, A. R., Cameron, D. R., Jones, C. P., 2003. Improvements to the representation of orography in the Met Office Unified Model. Quarterly Journal of the Royal Meteorological Society 129, 1989–2010.

Wergen, W., 1989. Normal mode initialization and atmospheric tides. Quarterly Journal of the Royal Meteorological Society 115, 535–545.

Wu, D. L., Hays, P. B., Skinner, W. R., 1995. A least squares method for spectral analysis of space-time series. Journal of the Atmospheric Sciences 52, 3501–3511.

Zhang, X., Forbes, J. M., Hagan, M. E., Russell III, J. M., Palo, S. E., Mertens, C. J., Mlynczak, M. G., 2006. Monthly tidal temperatures 20–120 km from TIMED/SABER. Journal of Geophysical Research 111, A10S08, doi:10.1029/2005JA011504.

Zhu, X., Yee, J.-H. Yee, Talaat, E. R., Mlynczak, M., Gordley, L., Mertens, C., Russell III, J. M., 2005. An algorithm for extracting zonal mean and migrating tidal fields in the middle atmosphere from satellite measurements: Applications to TIMED/SABERmeasured temperature and tidal modeling. Journal of Geophysical Reserch 110, D02105, doi:10.1029/2004JD004996.